B.Tech Project Report

Graphene: Theoretical Studies and Experimental Investigations

under the guidance of

(Dr. Sankalpa Ghosh) (Dr. Manish Sharma)

Submitted By:
Nupur Gupta
(2004PH10613)

Department of Engineering Physics
Indian Institute of Technology, Delhi
May 2008

Contents

Acknowledgements

I would like to express my sincere gratitude to my supervisors Dr. Sankalpa Ghosh & Dr. Manish Sharma for providing their invaluable guidance, comments and suggestions throughout the course of the project. I would specially thank Dr. Sankalpa Ghosh for constantly motivating me to work harder and Dr. Manish Sharma for getting me the HOPG samples.

Also I would like to thank Mr. S. Vidyananda for his assistance in the HRTEM imaging, Mr. Sandeep Sharma for his help during the preparation of the sample, Mr. Mandeep Singh for providing me an overview of the TEM image processing software Digital Micrograph.

Introduction

Graphenes are 2-D graphite layers a few monolayer thick. They comprise of hexagonal layers of C atoms arranged in honey-comb lattice. The existence of graphene as a single 2-D layer is a cause of amazement for many theoreticians as it has been believed for long that single layers of 2-D structures of this kind cannot exist, on account of being thermodynamically unstable. They suggested that the thermal fluctuations in low-dimensional crystal lattices would give rise to divergent contributions and the displacement of the atom will become comparable with the atomic distances at finite temperatures and the structure will be lost. The reason for the existence of these 2-D layers of graphene is suggested to be some kind of 3-D warping which increases the elastic energy of the graphene but reduces the thermal fluctuation energy and above a certain temperature the total free energy can be minimized **[1]**.

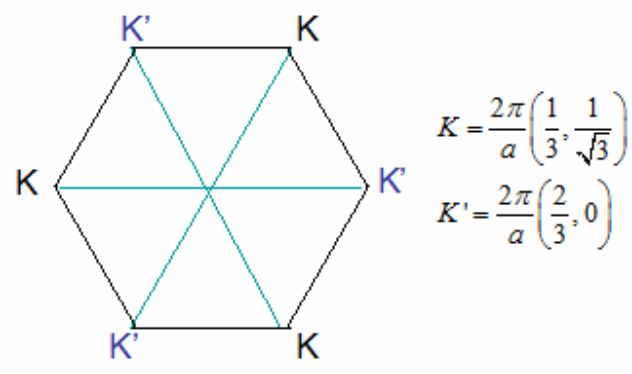

Fig1.1.The first brillouin zone of the 2-Dimensional graphene

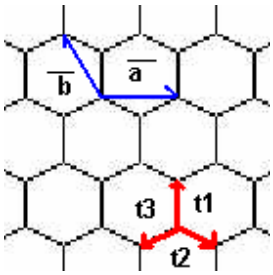

Fig1.2. The lattice structure of 2-D graphene with **a** and **b** primitive translation vectors and t_1, t_2, t_3 connect the nearest C atoms.

On account of their 2-D lattice structure they exhibit strange quantum mechanical and electronic properties. The low energy electrons (close to K and K' points as shown in **Fig1.1.)** inside the graphene behave as relativistic particles as is shown by their conciliation with the Dirac equation for relativistic particles. It has been rendered possible to imitate the quantum relativistic phenomena. Once the dispersion relation for graphene is obtained it becomes simpler to see the origin of these unique properties of graphene. Besides graphene exhibit strange quantum Hall Effect explained in terms of Berry's phase and which serves to give more insight into the electronic structure of graphene.

The dispersion relation for graphene is derived using the nearest neighbor tight binding model. The approach uses the Bloch type of wave function and the mutual interaction between the nearest neighbors to arrive at the following relation.

$$E_{\pm}(k) = \pm\gamma_o\sqrt{1+4\cos\frac{ak_x}{2}\cos\frac{\sqrt{3}ak_y}{2}+4\cos^2\frac{ak_x}{2}}$$

From the equation one can see that E(K) = E(K') = 0. Also near the K and K' points, we have.

$$E(K + k) = E(K'+ k) = \gamma(k_x^2+k_y^2)^{1/2}$$

This linear relationship between E and k in the vicinity of the points K and K' gives rise to relativistic nature of charge carriers in this region and decides the peculiar properties of graphene. Further description of electron behavior close to these points is given by the effective-mass equation or the k.p approximation model which furnishes the following Dirac equation in the region given by $|k|a_0<<1$ where a_0 is the lattice parameter and γ is proportional to the strength of interaction between nearest neighbors.

$$H = \gamma a_0\begin{pmatrix} 0 & k_x - ik_y \\ k_x + ik_y & 0 \end{pmatrix}$$

The project aims at investigating the unconventional electronic and structural properties of 2-dimensional lattice graphene. The known properties of graphene will be understood and explored further taking references from the existing literature through the simulation procedures as well as through experiments.

2. Analysis of graphene wavefunction & dispersion relation

In this section we present the result of simulations of the band diagram and the wavefunction of graphene 2-D lattice as a first step towards understanding its peculiar electronic properties. The simulation for the same is first performed for a 1-D lattice suitably modified to 2-D rectangular lattice and then for a hexagonal graphene lattice by the applicable translation of unit lattice vectors.

2.1 2-D rectangular lattice

We begin with the analysis of 2-D periodic lattice obeying Bloch periodicity equation. The wavefunctions as well as the periodic lattice potential is expanded as a 2-D Fourier series [**2**].

$$\psi(x) = \sum_{p,q} c_{p,q}e^{ipx+iqy}$$
$$U(x) = \sum_{G_x,G_y} U_{G_x,G_y}e^{iG_xx+iG_yy} \qquad (2.1\&2.2)$$

from which the corresponding coefficients of the Fourier series can be found out to be

$$U_{G_x,\,G_y} = \frac{1}{a}\int_0^a e^{-iG_x x - iG_y y} U(x,y)\,dxdy \qquad (2.3)$$

when we embed this solution in the Schrödinger equation

$$-\frac{\hbar^2}{2m}\nabla\psi(x,y) + U(x,y)\psi(x,y) = E\psi(x,y) \qquad (2.4)$$

we obtain the following eigen value equation

$$\left(-\frac{\hbar^2}{2m}(k_x - G)^2 + (k_x - G)^2 - E\right) c_{k_x - G,\,k_y - G} + \sum_{G'} U_{G' - G} * c_{k_x - G,\,k_y - G} = 0 \qquad (2.5)$$

The eigen value solution of the resulting 3-D matrix equation directly yields the E-k dispersion relationship as shown in **Fig2.1.1.** The code for the same is provided in **A.1**. Once the linear coefficients c(i,j) are calculated from the matrix equation by calculating its eigen values, the wavefunction Ψ(x,y) can be readily calculated by inserting into the equation. The code for the same is provided in **A.2.**

$$\psi(x,y) = \sum_{p,q} c(\mathrm{p},\mathrm{q})\exp(iqx + ipy) \qquad (2.1.1)$$

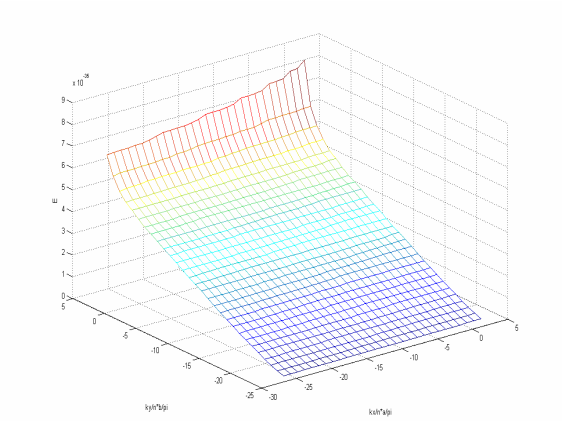

Fig2.1.1. The x and the y axis plotting the k values have been made dimensionless by multiplication with a factor of a/pi. Along the edges one can see a parabolic E-k relationship as expected for a 2D rectangular lattice.

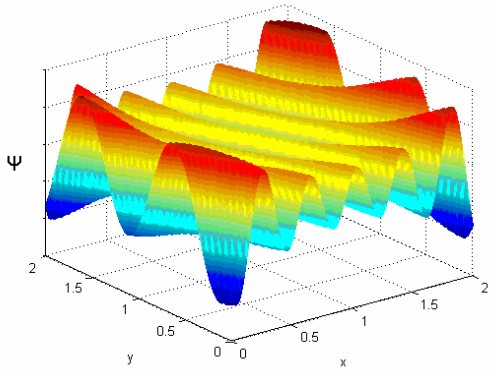

Fig 2.1.2 showing plot of the wavefunction Ψ(k,x) as a function of x and y for a given value of k. The lobes show the sinusoidal variation between two lattice points.

2.2 Graphene (Hexagonal lattice)

In this section the results for the 2D simulations of rectangular lattice have been scaled to a hexagonal lattice by transferring the axes in the basis space of hexagonal lattice defined by the unit lattice vectors a_1 & a_2 and the vectors K_1 & K_2 in the reciprocal lattice space as shown in **Fig2.2.1**

$$\hat{a}_1 = -a_0 \frac{\sqrt{3}}{2}\hat{x} + a_0 \frac{3}{2}\hat{y}, \quad \hat{a}_2 = a_0 \frac{\sqrt{3}}{2}\hat{x} + a_0 \frac{3}{2}\hat{y}. \tag{2.2.1}$$

$$\hat{k}_1 = \frac{2\pi}{a_0}\left(-\frac{\sqrt{3}}{3}\hat{x} - \frac{1}{3}\hat{y}\right) \qquad \hat{k}_2 = \frac{2\pi}{a_0}\left(\frac{\sqrt{3}}{3}\hat{x} - \frac{1}{3}\hat{y}\right) \tag{2.2.2}$$

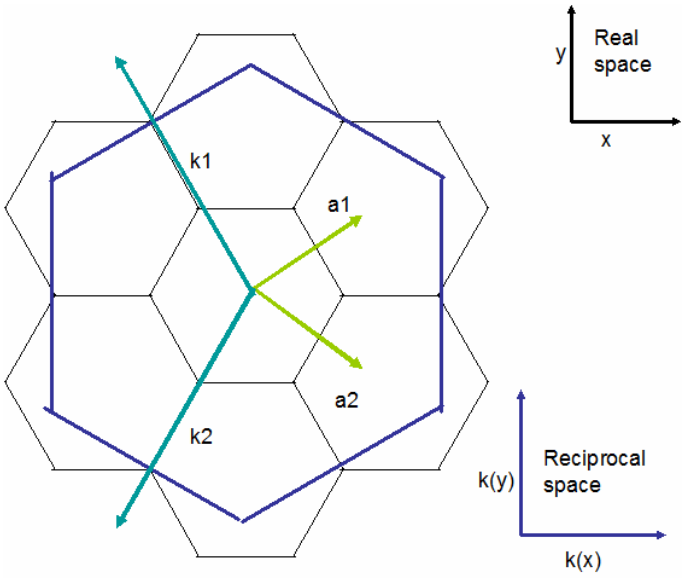

Fig2.2. 1. The unit cells of the crystal lattice are overlaid with the first Brillouin zone of the reciprocal lattice. Notice that the first Brillouin zone is scaled and rotated by 90^o

Using the LCAO method, the wavefunction of a unit lattice can be written as a linear combination of atomic orbitals [**3-4**] belonging to the C atoms comprising the unit cell as shown in **Fig2.2**.2.

$$\phi(r-R) = c_1\phi_1(r-R_1) + c_2\phi_2(r-R_2) \tag{2.2.3}$$

The wavefunction of the entire lattice will assume the Bloch form according to the following equation

$$|\psi> = \frac{1}{\sqrt{N}}\sum_R \exp(ik.R)\,|\phi_R> \tag{2.2.4}$$

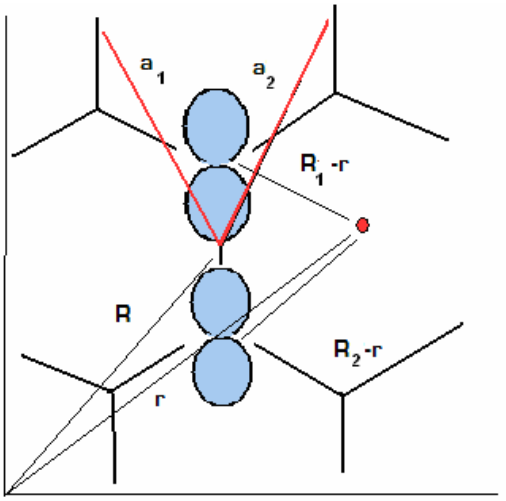

Fig2.2.2 showing the component wave functions of p_y orbitals corresponding to the A & B carbon atoms comprising a unit cell. The nearest neighbors shown by $R+a_1$,$R-a_1$,$R+a_2$,$R-a_2$ are considered in the approximation

Next we consider the interaction of this unit cell with the lattice.

$$H|\psi>=E|\psi> \tag{2.2.5}$$

If we consider each orbital individually, we get

$$\begin{aligned} <\phi_1|H|\psi>&=<\phi_1|E|\psi> \\ <\phi_2|H|\psi>&=<\phi_2|E|\psi> \end{aligned} \tag{2.2.6}$$

$$<\phi_1|H|\psi>=\frac{1}{\sqrt{N}}\sum_R \exp(ik.R)<\phi_1|H|\phi_R> \tag{2.2.7}$$

Here we make a tight binding approximation where the influence of non-neighboring atoms is overlooked.

$$\begin{aligned} &\sqrt{N}<\phi_1|H|\psi>=\exp(ik.0)<\phi_1|H|\phi_R>+\exp(ik.a_1)<\phi_1|H|\phi_{R-a1}> \\ &+\exp(ik.a_2)<\phi_1|H|\phi_{R-a2}>+\exp(-ik.a_1)<\phi_1|H|\phi_{R-a1}>+\exp(-ik.a_2)<\phi_1|H|\phi_{R-a2}> \end{aligned} \quad \ldots\ldots (2.2.8)$$

After some simplification we arrive at the following equations

$$\begin{aligned} c_1(\alpha-E)+c_2\beta(1+\exp(-ik.a_1)+\exp(-ik.a_2))=0 \\ c_2(\alpha-E)+c_1\beta(1+\exp(-ik.a_1)+\exp(-ik.a_2))=0 \end{aligned} \tag{2.2.9}$$

where α, β are overlap and hopping interaction respectively defined as

$$\alpha \equiv \langle \varphi_n | \hat{H} | \varphi_n \rangle$$
$$\beta \equiv \langle \varphi_n | \hat{H} | \varphi_m \rangle \quad \text{for n=1, 2.} \qquad (2.2.10)$$

The above equation can be put in matrix form as

$$\begin{pmatrix} \alpha - E & \beta(1+\exp(-ik.a_1)+\exp(-ik.a_2)) \\ \beta(1+\exp(-ik.a_1)+\exp(-ik.a_2)) & \alpha - E \end{pmatrix} \begin{pmatrix} c_1 \\ c_2 \end{pmatrix} = 0$$

2.2.1 Graphene band structure

By solving the above matrix for its eigen values the E-k dispersion relationship for the graphene is readily obtained. The matlab-code for the same is in **A.3**.

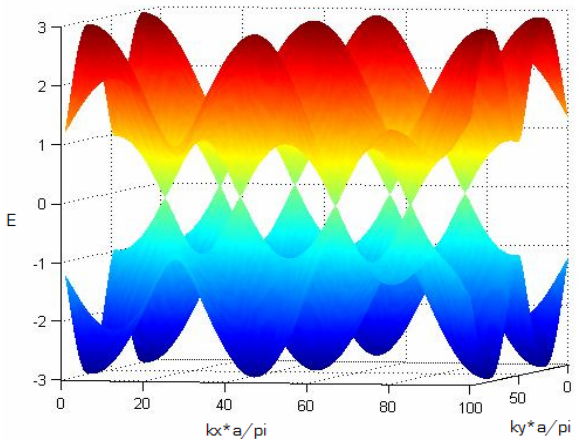

Fig2.2.1a. showing the linear E-k band relationship near the edges

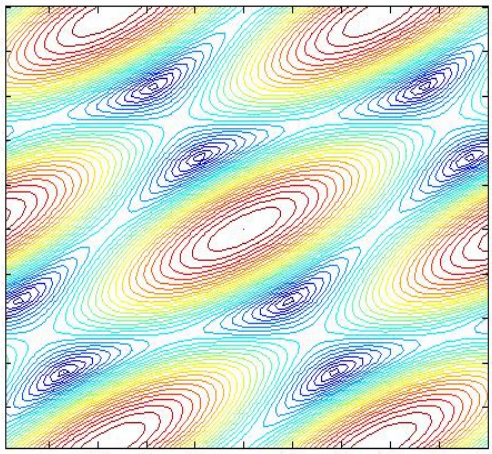

Fig2.2.1b. showing the contour plot of E-k diagram.

Thus we can see for a given value of k, there are two possible energy values forming conduction and valence band. The two bands touch each other at the K and K' points making graphene a zero band gap semiconductor. In the proximity of K and K' points the E-k diagram is linear whose Hamiltonian can be modeled as

$$\varepsilon = \frac{|h\mathbf{k}|}{2\pi} v_f$$

where v_f is the Fermi energy of the electron which is of the order of 10^6 m/s. The E-k relation for the charge carriers in an ordinary conductor is given by

$$\varepsilon = \frac{h^2 \mathbf{k}^2}{2\pi m}$$

The charge carriers in graphene thus mimic relativistic particles traveling at an effective speed of light following the Dirac equation. The mass of such carriers effectively vanishes around the valley points and thus they can rightly be called massless Dirac particles.

2.3.1 Graphene wavefunction

From the matrix equation, obtained by applying tight-bonding approximation on graphene unit lattice one can compute the linear coefficients c_1 and c_2 which describe the ratio in which the p_y orbital corresponding to A and B atom influence the wavefunction. Done in **A.3**.

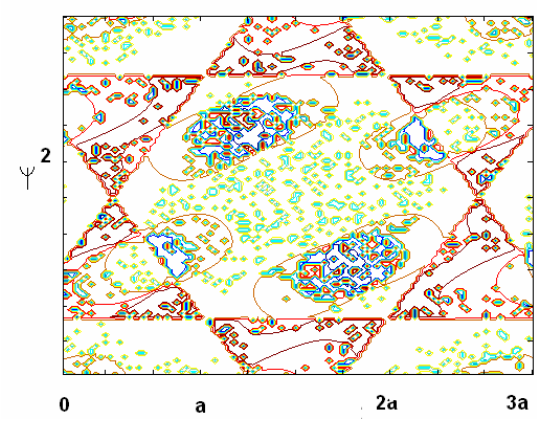

Fig2.3.1a. shows a contour plot of the wavef -unction due to sub-lattice A in the k- space.

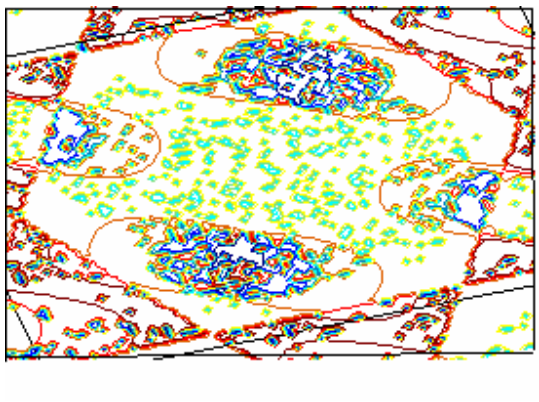

Fig2.3.1b.contour plot of the wavefunction due to sub-lat –tice B in the k space.

As shown in figure the individual wavefunctions of the sub-lattices A & B are conjugate of each other and together they produce a uniform probability density function around the corners of the hexagonal ring.

3. Analysis of graphene ribbons

So far the analysis has been done making approximations valid for infinite lattices, but the real solid-state devices that will be built out of graphene will be finite-sized and the electronic properties of the graphene will be modified under the influence of finite-size effects. The finite size effects will be exhibited in the quantized eigen states obtained from solving the problem within the legitimate boundary conditions. In this section we will see the finite size effects of graphene lattice on its electronic properties. As a result of finite size of lattice the continuum in conduction band gives way to confined states.

An additional quantization condition is introduced in the wavefunction calculation and the tight-binding approximation does not remain valid uniformly at all lattice points. It has

two distinct edges armchair and zig-zag differentiated by the arrangement of A & B type of atoms as shown in **Fig3.1**. The confinement along these edges results in different band structures which we will be explained in the later sections.

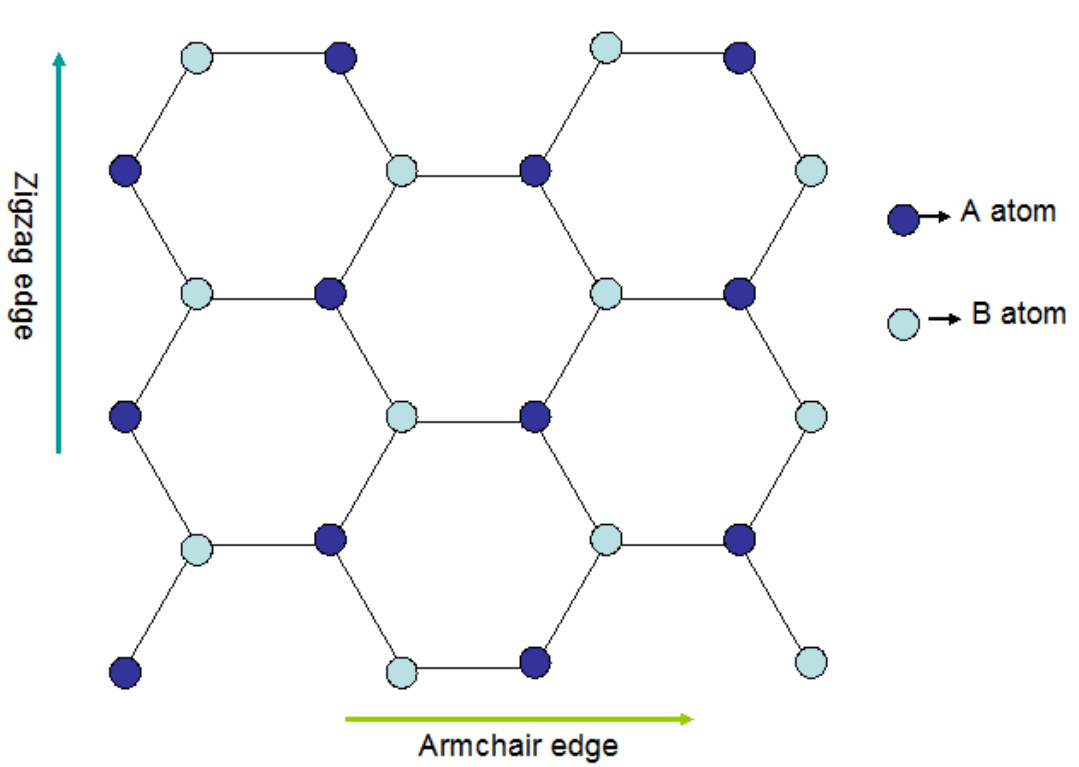

Fig3.1. The Zigzag edge comprises a single sublattice type whereas the armchair comprises both the sub-lattice types.

One can see from the **Fig3.1.** that the zigzag edge shown as dark circles in figure alternate in only a particular type of lattice atom i.e. to say that the wavefunction component due to the sub-lattice B vanishes completely at the zigzag edge. On the other hand, in the armchair edge which is lying perpendicular to the zigzag edge alternates in A and B type of atom. The boundary condition in this case thus will be satisfied by assuming that the two sub-lattices of graphene have equal weightings along the terminating edge .

3.1 **Confinement along zigzag direction**

Here we see the quantum mechanical treatment of the graphene monolayer confined along the direction perpendicular to the zigzag edge. We assume the coordinates axis to be placed so that the the zigzag edge lies along the y direction whereas the confinement is along the x direction. Consider a nano-ribbon of length L cut along the zigzag edge of graphene. Let the edge lying at x=0 comprise only B type of atoms and the edge along the

x = L comprises A type in our subsequent treatment. Then the boundary condition becomes [**5**].

$$\phi_A(x=0) = \phi'_A(x=0) = \phi_B(x=L) = \phi'_B(x=L) = 0 \qquad (3.1.1)$$

The two functions Φ and Φ' correspond to the K and K' points respectively. As stated earlier the states at the K and K' valley though qualitatively the same, are nonetheless inequivalent. The states differing in the location of K valleys are further subdivided by the A and B sub-lattice types. The Dirac equation inherently comprises of two orthogonal states known as Dirac spinors. In the case of Dirac particle graphene, these two spinors are contributed by the A and B sub-lattices and result in the Dirac like Hamiltonian of the single layer graphene. The rest of the tight-binding approximation will remain valid and we arrive at the following quantization condition. Consideration confinement along the x-axis, for each value of k_y . The 4- component graphene Hamiltonian is given as derived before

$$H = \gamma a_0 \begin{pmatrix} 0 & k_x + ik_y & 0 & 0 \\ k_x - ik_y & 0 & 0 & 0 \\ 0 & 0 & 0 & -k_x + ik_y \\ 0 & 0 & -k_x - ik_y & 0 \end{pmatrix} \qquad (3.1.2)$$

The associated wavefunction will be a 4-component eigen vector $\begin{bmatrix} \psi_A^K & \psi_B^K & \psi_A^{K'} & \psi_B^{K'} \end{bmatrix}$ where the subscript stands for the sub-lattice component of the wavefunction around the valley represented in the superscript. From the Hamiltonian it is clear that there is no interaction between the eigen-vector components belonging to different valleys. For the sake of simplification we therefore split the 4X4 Hamiltonian in two 2X2 eigen value equations.

$$\gamma a_0 \begin{pmatrix} 0 & k_x + ik_y \\ k_x - ik_y & 0 \end{pmatrix} \begin{pmatrix} \psi_A^K \\ \psi_B^K \end{pmatrix} = \varepsilon \begin{pmatrix} \psi_A^K \\ \psi_B^K \end{pmatrix}, \quad \gamma a_0 \begin{pmatrix} 0 & -k_x + ik_y \\ -k_x - ik_y & 0 \end{pmatrix} \begin{pmatrix} \psi_A^{K'} \\ \psi_B^{K'} \end{pmatrix} = \varepsilon \begin{pmatrix} \psi_A^{K'} \\ \psi_B^{K'} \end{pmatrix}$$

We now solve the above Hamiltonian for the K valley and the treatment of the other will be followed similarly. Solving the above Hamiltonian we obtain the following coupled linear differential equations.

$$\begin{aligned} \gamma a_0 (k_x + ik_y) \Psi_B^K &= \varepsilon \Psi_A^K \\ \gamma a_0 (k_x - ik_y) \Psi_A^K &= \varepsilon \Psi_B^K \end{aligned} \qquad (3.1.3)$$

The equations can be decoupled easily to obtain the plane wave solutions along the x as well as y direction. The new set of equation thus becomes

$$\begin{aligned} \gamma^2 a^2{}_0 (k_x + ik_y)(k_x - ik_y) \Psi_A^K &= \varepsilon^2 \Psi_A^K \\ \gamma^2 a^2{}_0 (k_x - ik_y)(k_x + ik_y) \Psi_B^K &= \varepsilon^2 \Psi_B^K \end{aligned} \qquad (3.1.4)$$

The k_x and the k_y operators are known to commute for this case yielding [k_x k_y]=0.

$$\left[k_x \quad k_y\right] = v\left(-i/\hbar\frac{\partial}{\partial x}\right)\left(-i/\hbar\frac{\partial}{\partial y}\right)-\left(-i/\hbar\frac{\partial}{\partial y}\right)\left(-i/\hbar\frac{\partial}{\partial x}\right) \tag{3.1.5}$$

$$=\left(-1/\hbar\frac{\partial^2}{\partial x\partial y}\right)+\left(1/\hbar\frac{\partial^2}{\partial y\partial x}\right)=0$$

The result zero comes from the following property that holds for the continuous functions.

$$\frac{\partial^2}{\partial y\partial x}=\frac{\partial^2}{\partial x\partial y}$$

Making use of the above fact, we can know solve our equations as follows.

$$\gamma^2 a^2{}_0(k_x k_x + ik_y k_x - ik_x k_y + k_y k_y)\Psi_A^K = \varepsilon^2\Psi_A^K$$

$$\gamma^2 a^2{}_0(k_x k_x - i[k_x k_y - k_x k_y] + k_y k_y)\Psi_A^K = \varepsilon^2\Psi_A^K$$

$$\gamma^2 a^2{}_0(k_x k_x - i\left[k_x \quad k_y\right] + k_y k_y)\Psi_A^K = \varepsilon^2\Psi_A^K$$

Making the substitution from above, this becomes

$$\gamma^2 a^2{}_0(k_x k_x + k_y k_y)\Psi_A^K = \varepsilon^2\Psi_A^K$$

$$\gamma^2 a^2{}_0\left\{\left(-i/\hbar\frac{\partial}{\partial x}\right)\left(-i/\hbar\frac{\partial}{\partial x}\right)-\left(-i/\hbar\frac{\partial}{\partial y}\right)\left(-i/\hbar\frac{\partial}{\partial y}\right)\right\}\Psi_A^K = \varepsilon^2\Psi_A^K$$

$$\frac{\gamma^2 a^2{}_0}{\hbar^2}\left(\frac{\partial^2}{\partial x^2}+\frac{\partial^2}{\partial y^2}\right)\Psi_A^K = \varepsilon^2\Psi_A^K$$

Similar equation will be obtained for the B sub-lattice component Ψ_B^K. Besides one can directly see the linear Dirac E-k relation from the above equation.

$$\varepsilon^2 = \frac{\gamma^2 a_0{}^2}{\hbar^2}\left(k_x{}^2 + k_y{}^2\right), \quad \varepsilon = \pm\frac{\gamma\, a_0}{\hbar}(k) \tag{3.1.6}$$

The above equation can be solved by the method of separation of variables where we will assume a solution of the form X(x).Y(y). Substituting this for Ψ_A^K we get

$$\frac{\gamma^2 a^2{}_0}{\hbar^2}\left(\frac{Y\partial^2 X}{\partial x^2}+\frac{X\partial^2 Y}{\partial y^2}\right)=\varepsilon^2 X(x)Y(y)$$

Dividing the whole equation by X(x).Y(y) we obtain

$$\frac{1}{X}\frac{\partial^2 X}{\partial x^2}+\frac{1}{Y}\frac{X\partial^2 Y}{\partial y^2}=\frac{\hbar^2\varepsilon^2}{\gamma^2 a^2{}_0}$$

We have a relation of the form f(x) + g(y) = constant. Or in other terms the equation can be expressed as F(x)=G(y). Clearly the LHS and RHS are independent of each other as x and y are independent variables. The solution therefore exists only for the case f(x) = constant and g(y) = constant. The equation now becomes

$$\frac{1}{X}\frac{\partial^2 X}{\partial x^2}=k(x)^2\ ,\quad \frac{1}{Y}\frac{X\partial^2 Y}{\partial y^2}=k(y)^2 \text{ such that } k(x)^2+k(y)^2=\frac{\hbar^2\varepsilon^2}{\gamma^2 a^2{}_0}$$

The solutions given by plane wave equations of the form $X(x)=X_0 e^{-ik(x)x}$, $Y(y)=Y_0 e^{-ik(y)y}$ seem to fit the physical picture quite well. For an infinite size lattice the wavefunction is a sinusoidal function of the space coordinates. The solution vector thus becomes of the following form

$$\begin{aligned}\Psi_A^K &= X_0 Y_0 e^{-ik(x)x-ik(y)y}\\ \Psi_A^{K'} &= X_0 Y_0 e^{-ik(x)x-ik(y)y}\end{aligned} \tag{3.1.7}$$

The remaining two components can be derived from these equations that we have encountered before

$$\gamma a_0(-k_x-ik_y)\Psi_A^K=\varepsilon\Psi_B^K$$
$$\gamma a_0(k_x+ik_y)\Psi_B^{K'}=\varepsilon\Psi_A^{K'}$$

For the case of finite sized lattices however, this plane wave solution is no more valid as it clearly fails to satisfy the boundary conditions. We will therefore look at the other solutions of the above equations in X(x) and Y(y). In the case, where the confinement is made along the x-direction the Y(y) retains the same $e^{ik(y)y}$ behavior. Let's begin with the most general solution of X(x).

$$X(x)=X_1 e^{ik(x)x}+X_2 e^{-ik(x)x} \text{ for } \psi_A^K \tag{3.1.8}$$

Now apply the boundary conditions for the zigzag edges, which require that the wavefunction for one sublattice vanishes completely at both the valleys [**7**] i.e.

$$\psi_A^K\ (x=0)=\psi_A^{K'}(x=0)=\psi_B^K(x=L)=\psi_B^{K'}(x=L)=0 \tag{3.1.9}$$

Applying the $\psi_A(x=0)=0$ && $\psi_B(x=L)=0$ condition we get, the following bounds on X_1 and X_2.

$$X_1 + X_2 = 0$$

Now from ψ_A^K we try to construct ψ_B^K using the following linear differential equation. $\gamma a_0(-k_x - ik_y)\Psi_A^K = \varepsilon\Psi_B^K$ which can be expanded into

$$\gamma a_0(i/\hbar\frac{\partial}{\partial x} + i/\hbar\frac{\partial}{\partial y})\Psi_A^K = \varepsilon\Psi_B^K \tag{3.1.10}$$

$$\varepsilon\Psi_B^K = \gamma a_0(i/\hbar\frac{\partial}{\partial x} + i/\hbar\frac{\partial}{\partial y})\left(X_1 e^{ik(x)x} + X_2 e^{-ik(x)x}\right) * e^{-ik(y)y} \tag{3.1.11}$$

$$\varepsilon\Psi_B^K = \gamma a_0(-ik(x)X_1 e^{ik(x)x} + ik(x)X_2 e^{-ik(x)x} - k(y)X_1 e^{-ik(x)x} - k(y)X_2 e^{-ik(x)x}) * e^{-ik(y)y}$$

$$\varepsilon\Psi_B^K(x=L) = \gamma a_0(-ik(x)X_1 e^{ik(x)L} + ik(x)X_2 e^{-ik(x)L} - k(y)X_1 e^{ik(x)L} - k(y)X_2 e^{-ik(x)L}) * e^{-ik(y)y} = 0$$

……(3.1.12)

$e^{ik(x)L}\left(-ik(x)-k(y)\right)X_1 + e^{-ik(x)L}\left(ik(x)-k(y)\right)X_2 = 0$ which yield the following relation using $X_1 + X_2 = 0$

$$\frac{ik(x)-k(y)}{ik(x)+k(y)} = e^{2ik(x)L} \tag{3.1.13}$$

The above equation sums up the quantization condition for the zigzag nano-ribbon of graphene. The real solution of k(x) exists for selective values of k(y) which gives rise to the k(y) vs. k(x) curve and from there the e vs. k(y) curve symmetric about the k(x)-k(y) plane given as below

$$\varepsilon^2 = \frac{\gamma^2 a_0^2}{\hbar^2}\left(k(x)^2 + k(y)^2\right) \tag{3.1.14}$$

The above plot has been obtained by finding the roots k(x) of the above equation for the input values k(y). The different sets of roots have then be plotted to give the branched structure of E-k diagram as shown in **Fig.3.1.2.** The code for the same is in **A.5**. The corresponding wave functions ψ_A^K, ψ_B^K.

$$\begin{pmatrix}\psi_A^K \\ \psi_B^K\end{pmatrix} = \begin{pmatrix}\sin(k(x)x) \\ \pm\frac{i}{\varepsilon}\{-k(x)\cos(k(x)) + k(y)\sin(k(x))\}\end{pmatrix} * X_0 Y_0 e^{-ik(y)y} \tag{3.1.15}$$

Here the value k(x) actually splits as k(x,n) to form various energy levels at the same value of k(y). The index n represents the number of nodes along the x-axis in the wave

function solution. The wavefunction for the zigzag edge for the states closest to the zero energy solution has been plotted in **Fig.3.1.1.** Plotted using the code in **A.6.**

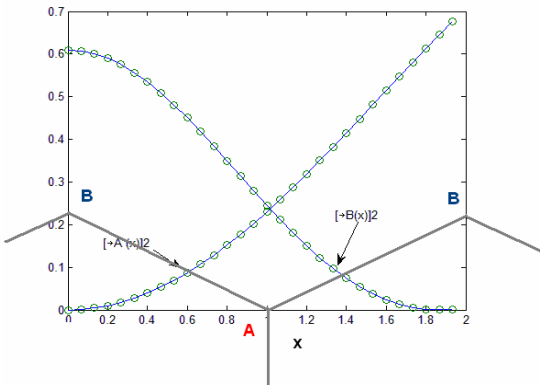

Fig3.1.1. Probability density variation between the two similar type of atoms along a zigzag edge superposed on the lattice structure

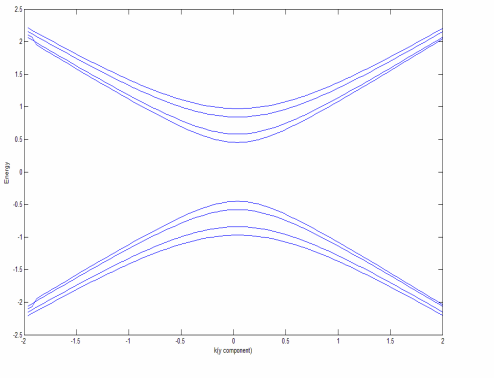

Fig3.1.2 E-k(y) quantization resulting from the confinement along the x-direction of a zigzag edge.

3.2 Confinement along armchair direction

The other prominent edge type seen in the hexagonal structure of graphene is the armchair edge in which the A and B sub-lattice atoms alternate along the edge. The atoms at the rightmost edge are at a distance of L+a/2 from the atoms at the leftmost edge. The appropriate boundary conditions therefore are [**4**].

$$\psi(x=0)=\psi'(x=0)$$
$$\psi(x=L+a_0/2)=\psi'(x=L+a_0/2)e^{i(K-K')(L+a0/2)} \qquad (3.2.1)$$

which suggest equal mixing of the wavefunction of the two sub-lattices at the edges. Applying the above boundary conditions, we obtain from the previous Hamiltonian equation

$$\psi_A^K(x=0)=\psi_A^{K'}(x=0)$$
$$\psi_B^K(x=0)=\psi_B^{K'}(x=0) \qquad (3.2.2)$$

The axis has again been adjusted such that the armchair edge lies along the y-axis whereas the confinement is along the x-direction.

Let us now begin with the following general solution as before.

$$X(x)=X_1e^{ik(x)x}+X_2e^{-ik(x)x} \text{ for } \psi_A^K$$

corresponding to which we already obtained

$$\varepsilon\Psi_B^K = \gamma a_0(-ik(x)X_1e^{ik(x)x} + ik(x)X_2e^{-ik(x)x} - k(y)X_1e^{-ik(x)x} - k(y)X_2e^{-ik(x)x}) * e^{-ik(y)y}$$

Similarly we assume a solution for $\psi_A^{K'}$ but with k(x) replaced by –k(x) as in the Hamiltonian of the K' valley.

$$X(x) = X_1e^{-ik(x)x} + X_2e^{ik(x)x} \text{ for } \psi_A^{K'} \tag{3.2.3}$$

corresponding to which we will obtain for the B sublattice

$$\varepsilon\Psi_B^{K'} = \gamma a_0(ik(x)X_1e^{-ik(x)x} - ik(x)X_2e^{ik(x)x} - k(y)X_1e^{ik(x)x} - k(y)X_2e^{ik(x)x}) * e^{-ik(y)y} \tag{3.2.4}$$

Applying the boundary conditions we now obtain in terms of equating $\Psi_B^{K'} = \varepsilon\Psi_B^K$,we obtain the following condition

$$(-k(x) + ik(y))X_1 + (k(x) + ik(y))X_2 = (-k(x) + ik(y))X_1 - (k(x) + ik(y))X_2 \tag{3.2.5}$$

which implies $X_2 = 0$ implying the following wavefunction vectors

$$\begin{pmatrix} \psi_B^K \\ \psi_B^{K'} \end{pmatrix} = X_1 \begin{pmatrix} e^{ik(x)x} \\ e^{-ik(x)x} \end{pmatrix} \tag{3.2.6}$$

Now if we apply the 2nd boundary condition at x=L we obtain the discretisation of k(x) as shown

$$\psi_B^K(x = L + a_0/2) = \psi_B^{K'}(x = L + a_0/2)e^{i(K-K')(L+a0/2)} \tag{3.2.7}$$

$$e^{2ik(x)(L+a0/2)} = e^{i(K-K')(L+a0/2)} \tag{3.2.8}$$

which gives us

$$k(x,n) = \frac{n\pi}{L + a_0/2} + \frac{2\pi}{3a_0} \tag{3.2.9}$$

So here we see unlike zigzag edge there is no dependence of k(x) on k(y). On the other hand we see that the value k(x)=0 will be achievable only for cases where L, the confinement length along the x-axis is of the particular form

$$L = \frac{(3n-1)}{2}a_0 \tag{3.2.10}$$

Depending upon this width, the ribbon might be insulating or conducting. In general for a length L=(3n +1) the armchair nano-ribbon is conducting and insulator otherwise. The energy also varies discontinuously with the nano-ribbon width. The electronic properties of armchair nano-ribbons depend strongly on their width as shown by the E-k

relationship for two distinct values of L as shown in **Fig.3.2.1**&**Fig.3.2.2.** The matlab codes for the same are in **A.7** and **A.8.**

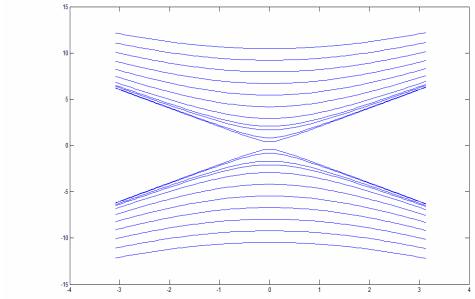

Fig3.2.1 For a different length L a non-metallic behavior is seen for confinement along an arm -chair edge.

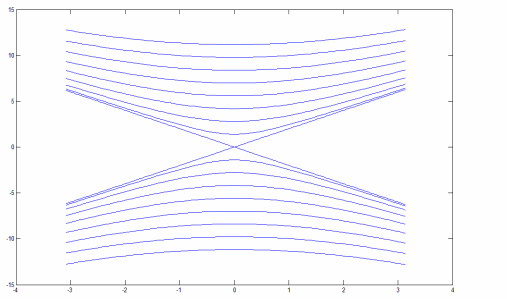

Fig.3.2.2A metallic behavior through a Dirac point is seen for an arm chair of a given edge.

One sees that between the x-axis points x=0 and x=L lying along the confined edge, there is a propagation constant of ΔK as can be seen from the eqn 3.2.1. Note that we have assumed ribbon to be extending infinitely along the y-axis with armchair configuration on the edge. In an armchair nano-ribbon, the intermixing of the two valley states result in a certain oscillation of wavefunction with period related to ΔK given by $2\Pi/\Delta$ as can be seen in simulation results in **Fig.3.2.2**. Plotted in **Fig.3.2.3, Fig.3.2.4** are two wavefunctions with different values of Length L of the nano-ribbon.

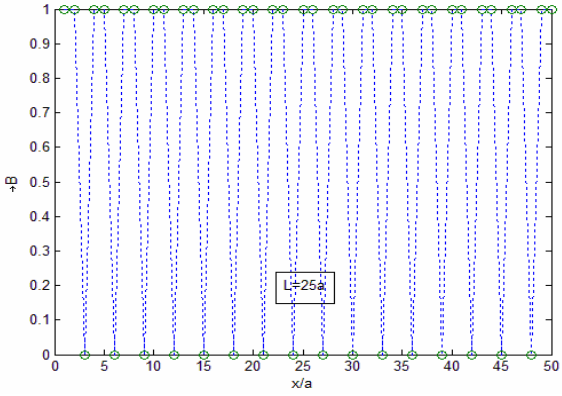

Fig.3.2.3 Ψ_B congruent to Ψ_A is plotted for a length L=25a. In this case the E-k diagram shows the presence of Dirac points which implies no effect of confinement and the wavefunction is non-fluctuating.

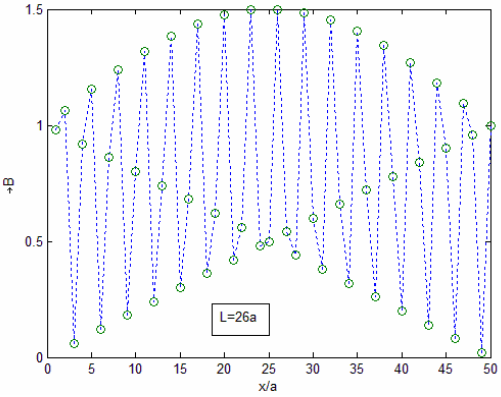

Fig3.2.4 The wavefunction shows fluctuation in accordance with the period expected for the valley mixing that were introduced to meet the boundary conditions.

4. Application of perpendicular magnetic field

In this section we consider, how the behavior of the graphene changes under the influence of a perpendicularly applied magnetic field. In the presence of a magnetic field, the free pi- electrons of graphene start executing a cyclotron motion perpendicular to the direction of applied field. For our case we apply a constant magnetic field along the z

direction which will consequently result in the in plane cyclotron motion of electrons. The B filed can be translated to the magnetic vector potential A [**6-11**].

$$B\hat{z} = \nabla X \vec{A} \tag{4.1}$$

resulting in the in-plane and components A_x, A_y of A. The effect of these components in the Hamiltonian of the graphene can be included by making the *Peirels substitution.*

$$p \longrightarrow p + i\nabla.A \tag{4.2}$$

Beginning from the Maxwell's equation $\varepsilon = -\frac{\partial A}{\partial t} - \nabla\phi$ along with the equation of motion of a charged particle in the magnetic field $F = e(\varepsilon + v * B)$ one arrives at the above substitution. For our case , we assume the y-component of the magnetic vector potential to be 0 which leaves us with the following expression for A(y).

$$A_y = B * x \tag{4.3}$$

Making the substitution mentioned above we arrive at these augmented expressions for p_x and p_y .

$$\begin{aligned} \kappa_x &= -i\hbar\frac{\partial}{\partial x} \\ \kappa_y &= -i\hbar\frac{\partial}{\partial x} + eBx \end{aligned} \tag{4.4}$$

These expressions will be substituted in the previous Hamiltonian to arrive at the graphene Hamiltonian in the presence of magnetic field. The rest of the treatment will also follow the same.

$$H = \frac{\gamma a}{\hbar}_0 \begin{pmatrix} 0 & \kappa_x + i\kappa_y & 0 & 0 \\ \kappa_x - i\kappa_y & 0 & 0 & 0 \\ 0 & 0 & 0 & -\kappa_x + i\kappa_y \\ 0 & 0 & -\kappa_x - i\kappa_y & 0 \end{pmatrix} \tag{4.5}$$

Note however that unlike in the previous case where $\begin{bmatrix} k_x & k_y \end{bmatrix} = 0$, the product $\begin{pmatrix} \pi_x & \pi_y \end{pmatrix}$ does not commutes to zero in this case. The solution of the equations therefore will not follow the same course.

$$\begin{bmatrix} \kappa_x & \kappa_y \end{bmatrix} = \left(-i/\hbar\frac{\partial}{\partial x}\right)\left(-i/\hbar\frac{\partial}{\partial y} - eBx\right) - \left(-i/\hbar\frac{\partial}{\partial y} - eBx\right)\left(-i/\hbar\frac{\partial}{\partial x}\right)$$

$$
\begin{aligned}
&= \left(-1/\hbar \frac{\partial^2}{\partial x \partial y}\right) + \left(1/\hbar \frac{\partial^2}{\partial y \partial x}\right) + \frac{i}{\hbar}\left(\frac{\partial (eBx)}{\partial x}\right) - \frac{ieBx}{\hbar}\left(\frac{\partial}{\partial x}\right) \\
&= \frac{ieB}{\hbar}\left(\frac{\partial}{\partial x}\right) + \frac{ieB}{\hbar} - \frac{i}{\hbar}\left(\frac{\partial (eBx)}{\partial x}\right) \\
&= \frac{ieB}{\hbar}
\end{aligned} \tag{4.6}
$$

On the contrary one can by doing another simplistic substitution sees that the new Hamiltonian is in agreement with the Hamiltonian of the simple harmonic oscillator. Lets define the new operators as follows [**6**].

$$
\begin{aligned}
a^{+} &= \frac{l}{\sqrt{2}}\left(\kappa_x - i\kappa_y\right) \\
a &= \frac{l}{\sqrt{2}}\left(\kappa_x + i\kappa_y\right)
\end{aligned} \tag{4.7}
$$

where l is defined as $l = \frac{\sqrt{eB}}{c}$. The wavefunction equations for ψ_A^K, ψ_B^K derived earlier can now be written making use of the notation as follows

$$
\begin{aligned}
\frac{2\gamma^2 a^2{}_0}{l^2} a a^{+} \Psi_A^K &= \varepsilon^2 \Psi_A^K \\
\frac{2\gamma^2 a^2{}_0}{l^2} a^{+} a \Psi_B^K &= \varepsilon^2 \Psi_B^K
\end{aligned} \tag{4.8}
$$

and similar equations for K' points. Besides, we have the following linear equations.

$$
\begin{aligned}
a^{+}\Psi_A^K &= \varepsilon\ \Psi_B^K & -a\ \Psi_A^{K'} &= \varepsilon\ \Psi_B^{K'} \\
a\Psi_B^K &= \varepsilon\ \Psi_A^K & -a^{+}\Psi_B^{K'} &= \varepsilon\ \Psi_A^{K'}
\end{aligned} \tag{4.9}
$$

for the K and the K' valleys respectively. Now we work out the analogy of this system with the Hamiltonian of the harmonic oscillator problem. The Harmonic oscillator Hamiltonian is given by the following equation

$$
H = \hbar\omega\left(a a^{+} - \frac{1}{2}\right) \tag{4.10}
$$

where the operators are such that

$$a = \alpha(\beta \hat{x} + i \hat{p})$$
$$a^{+} = \alpha(\beta \hat{x} - i \hat{p}) \tag{4.11}$$

We first seek to find the similarity between the operators defined as above for the Harmonic oscillator problem, with the similar operators defined for our magnetic field problem. For the case above we calculate the commutation product of the constituent operators x and p.

$$\left[\hat{x} \quad \hat{p}\right] = -ix/\hbar\left(\frac{\partial}{\partial x}\right) + i/\hbar\left(\frac{\partial}{\partial x}x\right)$$
$$= -ix/\hbar\left(\frac{\partial}{\partial x}\right) + i/\hbar\left(\frac{\partial}{\partial x} + x\right)$$
$$= \frac{i}{\hbar} \tag{4.12}$$

On the other side, the commutation product of the component operators of the a, a(+) operators defined for our problem is

$$\left[\kappa_x \quad \kappa_y\right] = \frac{ieB}{\hbar}$$

i.e. to say

$$\left[\kappa_x \quad \kappa_y\right] = c_0\left[\hat{x} \quad \hat{y}\right] \tag{4.13}$$

Hence we see that the a, a(+) operators occurring in the eigen value equation of harmonic oscillator problem and graphene in magnetic field problem are rather similar in construction The observation made above quite strengthens our proposition that the two problems bear semblance with each other. In the treatment that follows we try to solve the problem at hand by making use of the known solutions of the harmonic oscillator problem.

Now let's quickly go through various aspects of the harmonic oscillator solution. The eigen value equation is given by

$$H\psi = \hbar\omega(n + \frac{1}{2})\psi \tag{4.14}$$

which can be expanded as $\hbar\omega(aa^{+})\psi + \frac{\hbar\omega\psi}{2} = n\hbar\omega\psi + \frac{\hbar\omega\psi}{2}$ which simplifies to the following result $(aa^{+})_{HO}\psi = n\psi$ where the subscript HO stands for the a,a(+) operators in simple harmonic oscillator problem. We can now make use of this result for solving our equation $\frac{2\gamma^2 a^2{}_0}{l^2} aa^{+}\Psi_A^K = \varepsilon^2\Psi_A^K$. The effect of the operator composition a,a(+) will be similar as in the case of HO problem thus rendering the following solution.

$$H_1\psi = \frac{2\gamma^2 {a_0}^2}{l^2}(aa^+)\psi \tag{4.15}$$

$$H_1\psi = \left(\frac{2n\gamma^2 {a_0}^2}{l^2}\right)\psi \tag{4.16}$$

The RHS however for our case is not the energy eigen value rather it is a square of it giving a square root dependence of energy on the level n.

$$\left(\frac{2n\gamma^2 {a_0}^2}{l^2}\right)\psi_n \equiv \varepsilon^2\psi_n \tag{4.17}$$

$$\varepsilon_n = \pm\sqrt{2n}\,\frac{\gamma\, a_0}{l} \tag{4.18}$$

The solution that we have derived above is the Landau level solution [**12-16**] applicable to the systems subjected to a magnetic field. The index n stands for the nth Landau level. The corresponding functions ψ_n are the nth harmonic oscillator functions. One can see from the solution that it has a degeneracy of two for each index n. These two states physically correspond to the particle and the hole state The lowest Landau level (n=0) however does not possess any degeneracy. It is this property which lead to the observation of a novel type of Quantum Hall Effect in graphene **[12].** For these levels, the particle-hole conjugate of the wavefunctions are themselves.

The above solution is for ψ_A^K. The rest of the three components can be derived by making use of the coupled equations.

$$a^+\Psi_A^K = \varepsilon\ \Psi_B^K \tag{4.19}$$

Now, we make use of another result from the harmonic oscillator problem. The a(+) operator defined in the problem actually acts as an annihilation operator i.e. to say it takes a particle in nth state to the (n-1) the state.

$$a^+\Psi_n = c'\psi_{n-1} \tag{4.20}$$

which tells us that $a^+\Psi_{A,n}^K = c\Psi_{A,n-1}^K$. From which one can assign Ψ_B^K the following solution.

$$a^+\Psi_B^K = c''\Psi_{A,n-1}^K \tag{4.21}$$

The other components can be assigned a similar solution as follows.

$$\begin{pmatrix}\Psi_A^{K'}\\ \Psi_B^{K'}\end{pmatrix} = \begin{pmatrix}-c'\psi_n^{HO}\\ c''\psi_{n-1}^{HO}\end{pmatrix} \tag{4.22}$$

There is one thing however that we have overlooked in the above treatment. In the corresponding treatment of the a,a(+) operators for the two problems we make the following transformation.

$$\hat{x} \longrightarrow \hat{p}_x$$
$$\hat{p} \longrightarrow \hat{p}_y \qquad (4.23)$$

Corresponding to this transformation, there is a translation of the axis along the x-direction which can be incorporated in our solution by making the following substitution.

$$x \to x - k_y l^2 \qquad (4.24)$$

Along the y axis, there is no component of the magnetic field vector A and the y component of the total wave-function retains its plane wave nature of the form $e^{ik(y)y}$.

4.1 Confinement in the presence of magnetic field (Zigzag edge)

Now we confine our system along one of the axis(x) such that the zigzag edge lies along the infinite axis(y). We assume x to be varying from –X/2 to X/2. We can apply the same boundary conditions that were there in the graphene ribbon in the absence of magnetic field which will alter our present wavefunctions [**7**].

The wavefunctions that we have derived above are Hermite polynomials (solution of the Harmonic oscillator) which include a term of the form

$$\psi(x) \alpha \, \mathrm{e}^{-\frac{\gamma^2 x^2}{2}} \qquad (4.25)$$

which implies that these functions are peaked around x=0. Following from which we can see that the wavefunctions in our case i.e.

$$\psi(x - k_y l^2) \alpha \, \mathrm{e}^{-\frac{\gamma^2 (x - k y l^2)^2}{2}} \qquad (4.26)$$

are peaked around the zeros of $(x - k_y l^2)$. Consequently we obtain the following condition

$$-L/2 < x - k_y l < L/2$$

which can be further generalized to

$$-L/2 < (K + k_y) l^2 < L/2$$

thus a bound arises on the values of k(y) which is decided by the x-extension of the sample. The boundary condition has become for this case

$$\psi_{\mathrm{B}}^{\mathrm{K}}(x = 0) = 0$$
$$\psi_{\mathrm{B}}^{\mathrm{K'}}(x = 0) = 0$$

and similarly for the other edge. But our solutions derived in the previous section have a non-vanishing component at x=0. To fix this thing up, we add a small perturbation function to our obtained solutions. Redefine the original functions as follows

$$\psi new_B^K(x) = \psi_n(x - k_y l^2) * \omega(x) \tag{4.27}$$

Such that the function w(x) →0 as x→0 and the function stays close to unity at higher values of x. A good choice of such a function could be

$$\omega(x)=(1-e^{-\lambda x}) \tag{4.28}$$

with vanishing value at x=0 and a relatively slow dependence on x at points away from the x=0 boundary. This function carefully incorporates our physical situation. Thus we have

$$\psi_{new}(x)\alpha e^{-(x-k_y l^2)^2/2}(1-e^{-\lambda x}) \tag{4.29}$$

which under certain approximation becomes

$$\psi_{new}(x)\alpha e^{-(x-(k_y-\lambda)l^2)^2/2l^2} \tag{4.30}$$

Corresponding to the change in the wavefunction, there will be a perturbation term in the Hamiltonian which will likewise effect the E-k behavior [**6**] in the proximity of the edge as shown in **Fig4.1.1** & **Fig4.1.2.** The corresponding matlab codes are in **A.8** and **A.9** respectively.

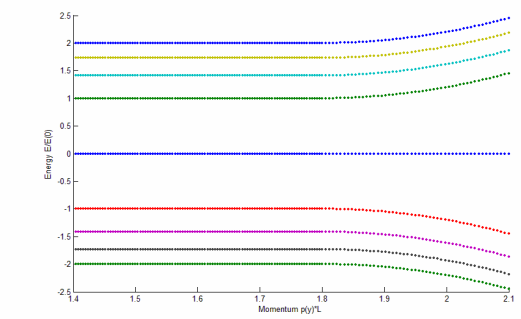

Fig4.1.1 Spectrum for the K valley, the n=0 Landau Level becomes a dipersionless mode near the edge.

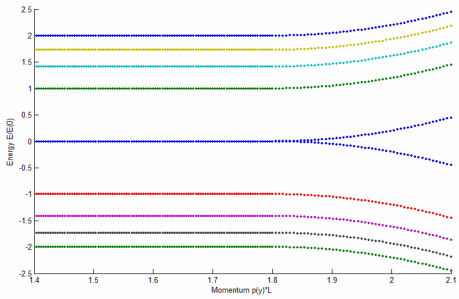

Fig4.1.2 Spectrum for the K' valley, the zeroth Landau level gives rise to two branches of dis -persing edge states.

Let us now define a new Hamiltonian H(edge) close to the edges which will operate on the wavefunction composed above to yield new eigen values .

4.2 Confinement in the presence of magnetic field (Armchair edge)

Now we study the confinement along the armchair. The terminating edge of the armchair nano-ribbon comprise of alternating A, B atoms. Hence the wave function should have an equal contribution from both the sub-lattices at the armchair edges which extend along the y-axis of our nano-ribbon. The boundary condition as already stated before is

$$\psi_A^K(x=0) = \psi_A^{K'}(x=0)$$
$$\psi_B^K(x=0) = \psi_B^{K'}(x=0) \qquad (4.2.1)$$

Now we have to alter our obtained wavefunctions so as to include the effect of above boundary conditions. If we revert back to our coupled equations

$$\gamma a_0(k_x + ik_y)\Psi_B^K = \varepsilon\Psi_A^K$$
$$\gamma a_0(k_x - ik_y)\Psi_B^{K'} = \varepsilon\Psi_A^{K'} \qquad (4.2.2)$$

we see that the effect of the above boundary condition is to add this constraint on the linear derivates of the A-sublattice components.

$$\frac{\partial\Psi_B^K}{\partial x} + i\frac{\partial\Psi_B^K}{\partial y} = \alpha\Psi_A^K \qquad (4.2.3)$$
$$\frac{\partial\Psi_B^K}{\partial x} + k_y\Psi_B^K = \alpha\Psi_A^K$$
$$\frac{\partial\Psi_B^K(x=0)}{\partial x} + k_y\Psi_B^K(x=0) = \alpha\Psi_A^K(x=0)$$

Similar analysis following from the second coupled equation yields

$$-\frac{\partial\Psi_B^{K'}}{\partial x} + i\frac{\partial\Psi_B^{K'}}{\partial y} = \alpha\Psi_A^{K'}$$
$$-\frac{\partial\Psi_B^{K'}}{\partial x} + k_y\Psi_B^{K'} = \alpha\Psi_A^{K'}$$
$$-\frac{\partial\Psi_B^{K'}(x=0)}{\partial x} + k_y\Psi_B^{K'}(x=0) = \alpha\Psi_A^{K'}(x=0) \qquad (4.2.4)$$

Now, noting the fact that k_y (K)= k_y (K') (from the Hamiltonian it is quite evident), we can arrive at the following condition.

$$-\frac{\partial\Psi_B^{K'}(x=0)}{\partial x} = \frac{\partial\Psi_B^K(x=0)}{\partial x} \qquad (4.2.5)$$

Now, we will deal with the situation by combining the two functions above in a single function as follows

$$\xi(x) = \theta(x)\psi_B^K(x) + \theta(-x)\psi_B^K(-x) \qquad (4.2.6)$$

where $\theta(x)$ is the step function, 1 for x>0, -1 for x<0 [**6**]. Now we look at the dependence of $\psi_B^{K,K'}$ on various parameters and the same dependence will be reflected in $\xi(x)$ after making some adjustments.

$$\gamma^2 a^2{}_0(\pi_x - i\pi_y)(\pi_x + i\pi_y)\Psi_B^K = \varepsilon^2\Psi_B^K$$
$$\gamma^2 a^2{}_0(\pi_x^2 + i(\pi_x\pi_y - \pi_y\pi_x) + \pi_y^2)\Psi_B^K = \varepsilon^2\Psi_B^K$$
$$\gamma^2 a^2{}_0\left(\frac{\partial^2}{\partial x^2} + i\left[\pi_x \quad \pi_y\right] + (k_y - eBx)\right)\Psi_B^K = \varepsilon^2\Psi_B^K \qquad (4.2.7)$$
$$\gamma^2 a^2{}_0\left(\frac{\partial^2}{\partial x^2} - eB/\hbar + (k_y - eBx)^2\right)\Psi_B^K = \varepsilon^2\Psi_B^K$$

Then substitute for B in terms of l^2 to obtain

$$\left(\frac{\partial^2}{\partial x^2} - 1/l^2 + (k_y - x/l^2)^2\right)\Psi_B^K = \frac{\varepsilon^2}{\gamma^2 a^2{}_0}\Psi_B^K \qquad (4.2.8)$$

We obtain the counterpart of this equation for $\psi_B^{K'}$. Now we look at our equation of $\xi(x)$ which becomes

$$\xi(x) = \begin{pmatrix} \psi_B^K(x) & x > 0 \\ \psi_B^{K'}(-x) & x < 0 \end{pmatrix} \qquad (4.2.9)$$

which now can be substituted by $\psi_B^K(x), \psi_B^{K'}(-x)$ to give the following equation in $\xi(x)$

$$\left(\frac{\partial^2}{\partial x^2} - 1/l^2 + (k_y - |x|/l^2)^2\right)\xi(x) = \frac{\varepsilon^2}{\gamma^2 a^2{}_0}\xi(x) \qquad (4.2.10)$$

We can make the function $\xi(x)$ obey the Schrödinger equation if we define a potential function U(x) as follows.

$$U(x) = \frac{l^2}{2}\left(\left(|x|/l^2 - k_y{}^2\right) - 1/l^2 + \frac{2}{l^2}\theta(\text{-x})\right) \qquad (4.2.11)$$

The corresponding Schrödinger equation will be

$$\left(-\frac{\partial}{\partial x^2} + U(x)\right)\psi(x) = \varepsilon'^2\psi(x) \qquad (4.2.12)$$

This double well potential as depicted in the potential function U(x) is as shown in **Fig.4.2.1(A.11).** There will actually be a hybridization corresponding to each of the Landau level, there will be a state corresponding to the left well as well as the right well. The particles lying in the left well which is minimized at a higher energy than the right well have higher energy eigen values for the Landau levels. As a result of the above

equation a perturbation term is added in the Hamiltonian around the edge states resulting in the E-k diagram shown in **Fig.4.2.2(A.12).**

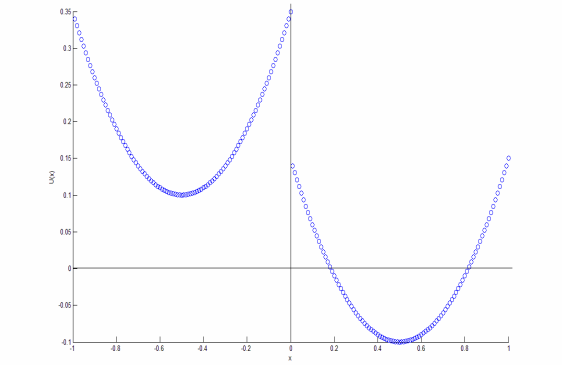

Fig4.2.1split potential function U(x) for an armchair Edge.

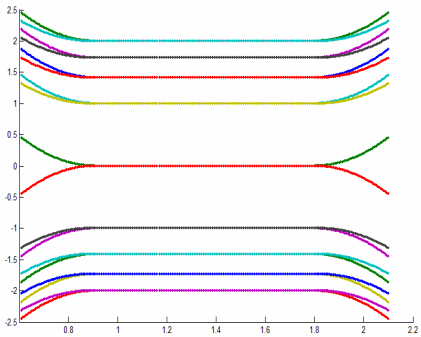

Fig4.2.2 the armchair boundary condition enha--nces the K, K' splitting in two edge modes.

3. Bilayer graphene

In this section we add an extra dimension to our analysis of graphene. We add another layer to the existing hexagonal plane. The two layers will try to align themselves with respect to each other in a lattice such as to minimize their potential energy in a closed packed arrangement. The hexagonal layer of spheres have a tendency to align themselves in a closed packed ABAB type arrangement where A atom of one layer fits in between the three B type atoms from the other layer as shown in **Fig.5.1**.Thus the bilayer graphene exhibits an ABAB type hexagonal close packing between the two layers.

Addition of another layer to graphene, gives rise to newer interactions in the model resulting from the inter-plane interactions. In this analysis we are going to refer to the unit cell atoms as A and B for one of the layer and A'' and B'' for the 2^{nd} layer. Also in the hexagonal packing arrangement we assume that B'' atoms in the 2^{nd} layer lie above the A atoms in first layer as shown in **Fig.5.1** thus forming the A-B'' dimer state. Such a dimer state results from some specific inter-molecular interactions between the two species. In the case of graphene the dimer state is confirmed experimentally by a fair estimate of the binding distance between the two atoms obtained using a planar functional model [**22**]. In addition to the in-plane interaction A-B we have A''-B", A-B'', B-A'' new interacting species in our model [**15-18**].

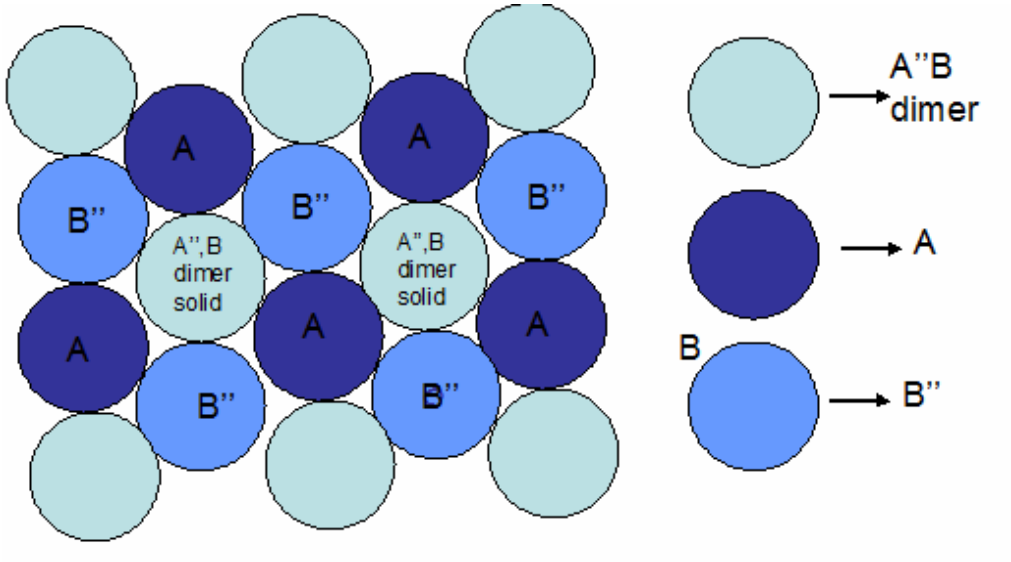

Fig5.1.bilayer structure where A,B are the atoms in the lower layer and A'',B'' are the atoms in the upper layer.

The A''-B'' interaction refers to the interaction between the A & B type of atoms in the 2nd layer quite analogous to the A-B type interaction in the bottom layer. Note that the fact that the A & B type of atoms are inequivalent is still preserved in the bilayer system as the unit cell construction still comprises of two atoms from a layer both of which bear an individual influence on the wavefunction at a nearby point. Now we analyze each of these interactions individually. The A-B interaction is similar as in our previous analysis given by the following Hamiltonian.

$$H_{A-B} = \nu \begin{pmatrix} 0 & k_x + ik_y \\ k_x - ik_y & 0 \end{pmatrix} \tag{5.1}$$

where ν stands for the strength of the interaction A-B and is proportional to γa_0 which in turn depends on t, the hopping parameter between the A and B atoms. Another A-B type interaction A''-B'' in the different plane will be similar. Next we consider the interaction between B-A''. Note that this interaction is different from the A-B'' interaction since the latter is a direct dimer state coupling between the two atoms, one located right on the top of the other. The former interaction on the other hand is an indirect interaction taking place between the layer of atoms following the same spatial arrangement as the A-B atoms but separated by a larger range.

$$\vec{r}_{B''-A} = \vec{r}_{B-A} + (\vec{z}_{B''} - \vec{z}_A) \tag{5.2}$$

so that the equivalent $a_0 = r_{B\text{-}A}$ becomes for this case

$$a_0^{'} = \sqrt{a_0^2 + c^2} \tag{5.3}$$

where c is the separation between the two layers. So that the unit vectors a_1 and a_2 can be modified as

$$\hat{a}_1' = -\frac{\sqrt{3}}{2}a_0'\hat{x} + \frac{3}{2}a_0'\hat{y}, \qquad \hat{a}_2' = \frac{\sqrt{3}}{2}a_0'\hat{x} + \frac{3}{2}a_0'\hat{y}$$

The set of reciprocal lattice vectors can then be generated as follows

$$\hat{k}_1' = \frac{2\pi}{a_0'}\left(-\frac{\sqrt{3}}{3}\hat{x} - \frac{1}{3}\hat{y}\right)$$

$$\hat{k}_2' = \frac{2\pi}{a_0'}\left(\frac{\sqrt{3}}{3}\hat{x} - \frac{1}{3}\hat{y}\right)$$

We see that the k-space is contracted as a result of the lengthening of the vector a_0. This inter-plane interaction therefore is only a weaker form of the intra-plane interaction A-B. Hence the resulting Hamiltonian is given by

$$H_{A''-B} = \nu_3\begin{pmatrix} 0 & k_x + ik_y \\ k_x - ik_y & 0 \end{pmatrix} \tag{5.4}$$

where the constant ν_3 is a measure of the strength of the interaction between the two atoms ($\nu_3/\nu << 1$).

Next we consider the direct inter-plane interaction resulting from the dimer state $\tilde{B-A}$. The interactions in this configuration can be expressed by the following Hamiltonian.

$$H_{B''-A} = \begin{pmatrix} 0 & \xi_1\gamma_1 \\ -\xi_1\gamma_1 & 0 \end{pmatrix} \tag{5.5}$$

where the constant γ_1 is a measure of the coupling existing in the dimer state and ξ_1 is just a symbol to account for later sign adjustments. This interaction is certainly stronger than the indirect interaction mentioned above. Now, we can pull together all these interactions to come up with a total Hamiltonian. We will disregard all other possible interactions.

$$H = \begin{pmatrix} 0 & \nu_3\pi & 0 & \nu\pi^+ \\ \nu_3\pi^+ & 0 & \nu\pi & 0 \\ 0 & \nu\pi^+ & 0 & \xi_1\gamma_1 \\ \nu\pi & 0 & -\xi_1\gamma_1 & 0 \end{pmatrix}, \quad \begin{aligned} \pi &= p_x + ip_y \\ \pi^+ &= p_x - ip_y \end{aligned} \tag{5.6}$$

The corresponding eigen value matrix of the above Hamiltonian comprise of the wavefunction vector $[\psi_A \quad \psi_{B''} \quad \psi_{A''} \quad \psi_B]$ describing the amplitude of electron waves on these coupled nearby sites.

Another thing that has not yet been taken into account is the possible potential difference between the two layers. This difference might result due to some intrinsic

property or due to the system being subjected to an external electric field. We therefore include a term +u/2 for the top layer and –u/2 for the bottom layer in our interaction.

$$H = \begin{pmatrix} u/2 & \nu_3\pi & 0 & \nu\pi^+ \\ \nu_3\pi^+ & -u/2 & \nu\pi & 0 \\ 0 & \nu\pi^+ & u/2 & \xi_1\gamma_1 \\ \nu\pi & 0 & -\xi_1\gamma_1 & -u/2 \end{pmatrix} \tag{5.7}$$

Having obtained the above Hamiltonian we now try to find the energy eigen values of this system. One approach is to straight forwardly diagonalize the above matrix to obtain its eigen values. A matlab method was invoked (#n) to calculate the same. The equation was solved numerically to obtain the ε vs. k plot as shown in **Fig.5.1.** The eigen values of the above matrix comes out to be

$$\varepsilon = \left[\frac{1}{2} \left(2\nu^2\pi^+\pi + \frac{u^2}{2} + \nu_3^2\nu^2 + \gamma_1^2 \pm 2 \left\{ \begin{matrix} \nu^2\pi^+\pi u^2 + \frac{\nu_3^4\pi^{+2}\pi^2}{4} - \frac{\nu^2\pi^+\pi\xi^2\gamma_1^4}{2} + \nu_3\pi^{+2}\pi^2 + \frac{\xi^4\gamma_1^4}{4} + \\ \xi^2\gamma_1^2\nu^2\pi^+\pi + \nu_3\pi^{+^3}\nu^2\xi\gamma_1 + \nu^2\pi^3\nu_3\xi_1\gamma_1 \end{matrix} \right\}^{1/2} \right) \right]^{1/2}$$

….(5.8)

which can be simplified by making the following substitutions

$$\begin{aligned} \xi^2 = 1, \xi^3 = \xi \\ \left[\pi \quad \pi^+ \right] = \pi\pi^+ - \pi^+\pi = 0 \\ \pi\pi^+ = p_x^2 + p_y^2 = p^2 \\ \pi^2\pi^{+^2} = \pi\pi\pi^+\pi^+ \\ = \pi\pi^+\pi\pi^+ \\ = p^2p^2 = p^4 \end{aligned} \tag{5.9}$$

let $\pi = p\cos\phi + ip\sin\phi$,then $\pi^3 = p\cos(3\phi) + ip\sin(3\phi)$, similarly $\pi^{+^3} = p\cos(3\phi) + ip\sin(3\phi)$ which implies

$$\pi^3 + \pi^{+^3} = 2p\cos(3\phi) \tag{5.10}$$

The equation above thus becomes

$$\varepsilon^2 = \frac{1}{2} \left(2\nu^2p^2 + \frac{u^2}{2} + \nu_3^2\nu^2 + \gamma_1^2 \pm 2 \left\{ \begin{matrix} \nu^2p^2u^2 + \frac{\nu_3^4p^4}{4} - \frac{\nu^2p^2\xi^2\gamma_1^4}{2} + \nu_3p^4 + \frac{\xi^4\gamma_1^4}{4} + \\ \xi^2\gamma_1^2\nu^2p^2 + 2\nu_3\nu^2\xi\gamma_1p^3\cos(3\phi) \end{matrix} \right\}^{1/2} \right)$$

…..(5.11)

which can be further simplified to

$$\varepsilon^2 = v^2 p^2 + \frac{u^2}{4} + \frac{v_3^2 v^2}{2} + \frac{\gamma_1^2}{2} \pm \left\{ v^2 p^2 (u^2 + \gamma^2 + v_3 p^2) + \frac{(v_3^2 p^2 - \gamma_1^2)^2}{4} + 2 v_3 v^2 \xi \gamma_1 p^3 \cos(3\phi) \right\}^{1/2}$$

From the above equation we see that the energy is dependent on the phase ϕ (in the momentum space) of the particle in addition to the magnitude of its momentum. The E-p diagram would therefore not be symmetric in the momentum space rather it will exhibit n nodes along the tangential direction. The value of n being decided by the no. of maximas of cos(3ϕ) between 0 and 2pi. There are 3 such maximas occurring at 0, 2pi/3,4pi/3. The picture can be seen in **Fig.5.2(A1.14)**. showing zeros at certain values of the phase in the p space.

Also note that there are two value of energy e corresponding to the momentum vector p. One of these values (+ve sign) is higher than the other. And corresponding to these two values will be their negative counterparts that add up to the total of four eigen values as shown in **Fig5.1(A1.13)**.This higher value results from the interaction taking place in B''-A dimer state (strong overhead interaction). The low energy bands on the other hand will correspond to the –ve sign and corresponds to the weaker interactions. Here we

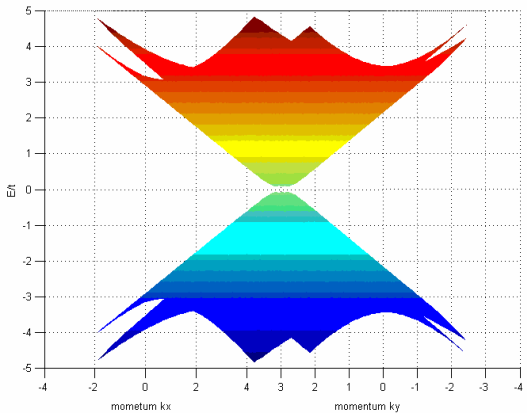

Fig5.1 E-k band showing the 4-level degeneracy.

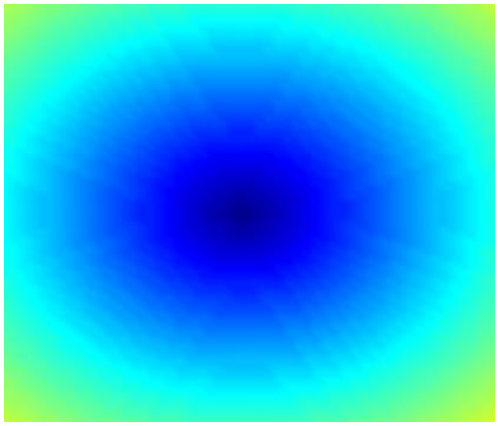

Fig5.2 contour plot of the E-k diagram shown on the left showing asymmetry in the tangent--ial direction.

approximate the dispersion relation close in the low energy regime making use of the following…. $v_3 << v$ so that the terms including v_3 and its higher powers can be neglected. Also the energy range is chosen such that the $|\varepsilon| > u$ (inter-layer potential). Under these approximations we have

$$\varepsilon_-^2 = v^2 p^2 + \frac{\gamma_1^2}{2} - \left\{ v^2 p^2 (\gamma^2) + \frac{(-\gamma_1^2)^2}{4} \right\}^{1/2}$$
$$= \frac{\gamma_1^2}{4} \left(\frac{4v^2 p^2}{\gamma_1^2} + 2 - \left\{ \frac{4v^2 p^2}{\gamma_1^2} + 1 \right\}^{1/2} \right) \qquad (5.12)$$
$$= \frac{\gamma_1^2}{4} \left(\left\{ \frac{4v^2 p^2}{\gamma_1^2} + 1 \right\}^{1/2} - 1 \right)^2$$

which yields the following low energy dispersion relation

$$\varepsilon_- = \pm \frac{\gamma_1}{2} \left(\left\{ \frac{4v^2 p^2}{\gamma_1^2} + 1 \right\}^{1/2} - 1 \right) \qquad (5.13)$$

Now, if we look at the energy spectrum derived above for the (-ve) branch, we can infer in the high momentum regime approximates to a linear interpolation between E & p which translates to a quadratic spectrum at lower values of p. For large values of p, this becomes

$$\varepsilon_- = \pm \frac{\gamma_1}{2} \left(\frac{2v p}{\gamma_1} \right) = \pm v p \qquad (5.14)$$

and for smaller values this becomes

$$\varepsilon_- = \pm \frac{\gamma_1}{2} \left(\frac{2v^2 p^2}{\gamma_1^2} \right) = \pm \frac{v^2 p^2}{\gamma_1} \qquad (5.15)$$

From this equation we can calculate the effective mass of for electrons following this equation (close to Fermi energy) from the definition

$$m_{eff} = p / \frac{\partial \varepsilon_-}{\partial p} \qquad (5.16)$$

The effective mass then comes out to be

$$\frac{\partial \varepsilon_-}{\partial p} = \pm \frac{\gamma_1}{2} . \frac{1}{2} . \left\{ \frac{4v^2 p^2}{\gamma_1^2} + 1 \right\}^{-1/2} . \frac{8v^2 p}{\gamma_1^2}$$
$$= \pm \left\{ \frac{4v^2 p^2}{\gamma_1^2} + 1 \right\}^{-1/2} . \frac{2v^2 p}{\gamma_1} \qquad (5.17)$$

We know that for a 2-D gas the density N (of free charge carrier) is related to the phase space area as. Consider a two dimensional p-space with axes p_x and p_y. We want to calculate the number of allowable modes for a certain value of momentum p. That is we want to calculate the number of modes lying within a rectangle of size p_x and p_y.

$$N = \frac{p^2}{Area/node} \tag{5.18}$$

The value Area/node can be found out by making use of the following quantization condition for confined modes as follows:

$$k_x = \frac{n\pi}{L_x}, \quad k_y = \frac{n\pi}{L_y}, \quad \Delta k_x = \frac{\pi}{L_x}, \quad \Delta k_y = \frac{\pi}{L_y} \tag{5.19}$$

correspondingly $\Delta p_x = \frac{\hbar\pi}{L_x}$, $\Delta p_y = \frac{\hbar\pi}{L_y}$, from which the area of a solution in the p space can be calculated as

$$\Delta p_x \Delta p_y = \frac{\hbar^2\pi^2}{L_x L_y} \tag{5.20}$$

$$\Delta p_x \Delta p_y = \frac{\hbar^2\pi^2}{A}$$

$$N = \frac{p^2}{\Delta p_x \Delta p_y} = \frac{p^2}{\hbar^2\pi^2/A}, \; N' = \frac{N}{A} = \frac{p^2}{\hbar^2\pi^2} \tag{5.21}$$

so that the m(eff) becomes

$$\frac{\partial \varepsilon_-}{\partial p} = \pm\left\{\frac{4\nu^2\pi\hbar^2 N}{\gamma_1^2} + 1\right\}^{-1/2} . \frac{2\nu^2 p}{\gamma_1}$$

$$m_{eff} = \frac{p}{\pm\left\{\frac{4\nu^2\pi\hbar^2 N}{\gamma_1^2} + 1\right\}^{-1/2} . \frac{2\nu^2 p}{\gamma_1}}$$

$$= \pm\frac{\gamma_1}{2\nu^2}\sqrt{\frac{4\nu^2\pi\hbar^2 N}{\gamma_1^2} + 1} \tag{5.22}$$

Thus, unlike the case of Dirac fermions in single layer graphene, the electrons in bilayer have a non-zero effective mass resulting from the low-energy interlayer interaction. This is one of the marked difference between single and bilayer graphene. We see that the mass is directly proportional to the free-carrier charge density inside the sample. As the doping concentration N increases, the resultant effective mass increases for values nearer to the center of Brillouin zone (low-energy values).

For the time being, we will take the interlayer (u) potential to be zero as it will lie along the diagonal and will not alter our solution. We can set it to non-zero at a later stage in case it is required. Also we neglect the indirect interaction (v_3) taking place between

these two atoms as its magnitude is very small compared to the rest of the interactions γ and v.

Now, we will try to model the Hamiltonian applicable for low-energy electrons which allows us to deal with the bilayer graphene in the low-energy regime. For this purpose we will need to extract out the terms corresponding to the low-energy interactions. That is, we concentrate on the interaction between A''-B atoms by trying to project the 4X4 matrix to a 2X2 inter-dependency matrix between these two electron wave functions i.e. we want to find a 2X2 matrix H' such that it corresponds to the solution of following equations:

$$H' = \begin{pmatrix} \hat{\alpha} & \hat{\beta} \\ \hat{\gamma} & \hat{\delta} \end{pmatrix} \quad , \quad \begin{aligned} \hat{\alpha}\psi_A + \hat{\beta}\psi_{B'} &= \varepsilon\psi_A \\ \hat{\gamma}\psi_A + \hat{\delta}\psi_{B'} &= \varepsilon\psi_B \end{aligned} \tag{5.23}$$

where we know that the diagonal terms corresponding to A-A and B-B index is zero since the potential of both the layers has been set to null. To achieve this goal we can directly expand the full 4X4 Hamiltonian H into four linear equations and bring it in the format desired as stated above. But this will rather be a cumbersome process, so we will make use of a more sophisticated technique of Green's functions for solving our equations. Consider a differential equation of the form

$$\hat{L}\,g(x) = f(x) \tag{5.24}$$

where L is some linear operator, f is a known function and g is the function to be solved. The green function G are defined for any linear operator L as follows

$$\hat{L}\,G(x,s) = \delta(x-s) \tag{5.25}$$

where $\delta(x-x_0)$ is the Dirac delta function. Making use of the above we can now rewrite our equation as

$$\begin{aligned} &\hat{L}\,G(x)\,f(s) = \delta(x-s)\,f(s) \\ &\int \hat{L}\,G(x)\,f(s)ds = \int \delta(x-s)\,f(s)ds = f(x) = \hat{L}\,g(x) \end{aligned} \tag{5.26}$$

now since the operator L is linear and is a function of x only, it can be brought out of the integral to yield the following result:

$$g(x) = \int G(x)\,f(s)ds \tag{5.27}$$

which allows us to calculate the function g(x) in terms of the obtained function G(x). In our case all the elements of the Hamiltonian matrix are linear operators. Hence the Green function methodology is applicable. However we are interested only in the Green function in the low-energy region, we divide the system into 4-sub parts, corresponding to different interactions. Let H_{11} refer to the top-left block corresponding to the low-energy inter-plane interaction in the complete Hamiltonian H derived above. Similarly

extract out H_{12}, H_{21}, H_{22} and write down the above Hamiltonian in block matrix notation such that

$$H = \begin{pmatrix} H_{11} & H_{12} \\ H_{21} & H_{22} \end{pmatrix} \tag{5.28}$$

The corresponding Greens function G constructed as

$$G = \begin{pmatrix} G_{11} & G_{12} \\ G_{21} & G_{22} \end{pmatrix}, \qquad G = (H - \varepsilon)^{-1} \tag{5.29}$$

is derived from the Hamiltonian H itself in a manner so that the block G_{11} can independently represent the interaction between the concerned wave functions as depicted in the total Hamiltonian H_1[22]. This is achieved by including the effect of the remaining terms on the subject wave functions in the terms of G itself. We try to obtain the solution for the block G_{11}. The method is as follows: (from definition)

$$\begin{aligned} G &= \begin{pmatrix} (H_{11} - \varepsilon)^{-1^{-1}} & H_{12} \\ H_{21} & (H_{22} - \varepsilon)^{-1^{-1}} \end{pmatrix}^{-1} \\ &= \begin{pmatrix} G'_{11^{-1}} & H_{12} \\ H_{21} & G'_{22^{-1}} \end{pmatrix}^{-1} \\ &= \frac{1}{G_{11^{-1}} G_{22^{-1}} - H_{12} H_{21}} \begin{pmatrix} G_{22^{-1}} & -H_{21} \\ -H_{12} & G_{11^{-1}} \end{pmatrix} \end{aligned} \tag{5.30}$$

so that we obtain

$$\begin{aligned} G_{11} &= \frac{G'^{-1}_{22}}{G'^{-1}_{22} G'^{-1}_{11} - H_{21} H_{12}} \\ &= G'_{11}(1 - G'_{11} H_{12} G'_{22} H_{21})^{-1} \end{aligned} \tag{5.31}$$

From above, by taking the matrix inverse, we get G'^{-1}_{11} to be

$$G_{11^{-1}} = (1 - G'_{11} H_{12} G'_{22} H_{21}) G'_{11^{-1}} \tag{5.32}$$

Now we try to eliminate G'_{11} from the above equation by substituting back in terms of H_{11}($G'_{11^{-1}} = H_{11} - \varepsilon$)

$$G_{11^{-1}} = G'_{11^{-1}} - G'_{11^{-1}} G'_{11} H_{12} G'_{22} H_{21}$$

$$G_{11}^{-1} + \varepsilon = H_{11} - H_{12} G'_{22} H_{21} \tag{5.33}$$

Now we expand $G_{22} = (H_{22} - \varepsilon)^{-1}$ under the above mentioned assumptions on u and v_3. For the low energy band analysis we neglect powers of p greater than equal to 2. The obtained result is then substituted in the equation written above to obtain the Greens function G_{11}. A matlab procedure was written to perform the above-mentioned matrix manipulations which yielded the following matrix for G_{11}.

$$G_{11} = \begin{pmatrix} 0 & -\frac{1}{2}\left(v^2\pi^{+^2}\sqrt{\xi^2\gamma_1^2 + 4v^2p^2}\right) \\ -\frac{1}{2}\left(v^2\pi^2\sqrt{\xi^2\gamma_1^2 + 4v^2p^2}\right) & 0 \end{pmatrix} \tag{5.34}$$

The matrix obtained above is the solution matrix H' we talked about earlier. The diagonal elements corresponding to the potential energy term are zero as expected whereas the off-diagonal terms representing the interaction between A'' and B bear an influence of both the inter-plane direct dimer interaction as well as the in-plane A-B interaction. We thus have H' in the desired form

$$H' = \begin{pmatrix} \hat{\alpha} & \hat{\beta} \\ \hat{\gamma} & \hat{\delta} \end{pmatrix}$$

Further simplification can be done by substituting m_{eff} as derived in equation 5.22 for the constant term in the above matrix to obtain

$$H' = -\frac{1}{2m_{eff}} \begin{pmatrix} 0 & \pi^{+^2} \\ \pi^2 & 0 \end{pmatrix} \tag{5.35}$$

We have thus arrived at a compact Hamiltonian which captures the properties of particles lying in the low energy band. Note, however that the notion of the sub-lattice in this system has now changed to the atom A from the lower layer and the atom B'' from the 2nd layer as opposed to A & B in the same layer in the single layer case.

On the other hand if we consider the +ve sign in the obtained E-k in the eq. we get an equation in E and p which is rather cumbersome to look at. We don't concern ourselves with the high-energy bands corresponding to the +ve sign in this report.

5.1 Magnetic field applied to a bilayer

Now we apply a perpendicular magnetic field to the bilayer graphene. The conventions are similar as in previous analysis. As earlier the first step will be to do the Peierls

substitution in the p(y) operator giving to include eBx/c component. The eigen value equation for this case becomes

$$\begin{aligned} \pi^{+^2}\psi_B &= -2m_{eff}\varepsilon\psi_A \\ \pi^2\psi_A &= -2m_{eff}\varepsilon\psi_B \end{aligned}, \qquad \begin{aligned} \pi &= \pi_x + i\pi_y \\ \pi^+ &= \pi_x - i\pi_y \end{aligned}, \qquad \begin{aligned} \pi_x &= p_x \\ \pi_y &= p_y + eBx \end{aligned} \tag{5.1.1}$$

Decoupling the above equations we obtain

$$\begin{aligned} \pi^2\pi^{+^2}\psi_B &= 4m_{eff}^2\varepsilon^2\psi_A \\ \pi^{+^2}\pi^2\psi_A &= 4m_{eff}^2\varepsilon^2\psi_B \end{aligned} \tag{5.1.2}$$

Now let us look at the following simplification

$$\begin{aligned} \pi\pi^+ &= (\pi_x + i\pi_y)(\pi_x - i\pi_y) \\ &= \pi_x^2 + \pi_y^2 - i\left[\pi_x \quad \pi_y\right] \end{aligned} \tag{5.1.3}$$

$$\begin{aligned} &= \pi_x^2 + \pi_y^2 - i\frac{-ieB}{\hbar} \\ &= \pi_x^2 + \pi_y^2 - \frac{eB}{\hbar} \end{aligned} \tag{5.1.4}$$

similarly, $\pi^+\pi = \pi_x^2 + \pi_y^2 - \frac{eB}{\hbar}$ so that we can make the following substitution

$$\pi^+\pi = \pi\pi^+ + \frac{2eB}{\hbar} \tag{5.1.5}$$

in $\pi^2\pi^{+^2}$.

$$\begin{aligned} \pi^2\pi^{+^2} &= \pi\pi\pi^+\pi^+ \\ &= \pi\left(\pi^+\pi - \frac{2eB}{\hbar}\right)\pi^+ \\ &= \pi\pi^+\pi\pi^+ - \frac{2eB}{\hbar}\pi\pi^+ \end{aligned} \tag{5.1.6}$$

Now if we represent the operator composition $\pi\pi^+$ by H_{temp}, we have our equation in the following form.

$$\left[H_{temp}H_{temp} - \frac{2eB}{\hbar}H_{temp}\right]\psi_A = 4m_{eff}^2\varepsilon^2\psi_A \tag{5.1.7}$$

The solution of the operator H_{temp} is already derived in the previous section so here we will directly use the following result.

$$H_{temp}\psi_n(x) = n\hbar\omega\psi_n(x) \tag{5.1.8}$$

where $\psi_n(x)$ is the nth Hermite polynomial. We will see that the solution for the above equation once again is similar to the Harmonic oscillator solution. So that if we apply $\psi_n(x)$ as an eigen function to the above Hamiltonian we get

$$\left[H_{temp}H_{temp}-\frac{2eB}{\hbar}H_{temp}\right]\psi_n = H_{temp}\left(n\hbar\omega\psi_n\right)-\frac{2eB}{\hbar}n\hbar\omega\psi_n$$

$$= n^2\hbar^2\omega^2\psi_n-\frac{2eB}{\hbar}n\hbar\omega\psi_n \qquad (5.1.9)$$

Note that, we have earlier defined the equivalent ω as the cyclotron frequency of the motion of charged particle in a magnetic field , $\omega' = 2eB/\hbar^2$ for our situation . So the simplification becomes

$$\left[H_{temp}H_{temp}-\frac{2eB}{\hbar}H_{temp}\right]\psi_n = n(n-1)\hbar^2\omega'^2\psi_n \qquad (5.1.10)$$

From above we can derive the Landau level energy spectrum of the electrons in a bilayer graphene in the presence of a magnetic field.

$$4m_{eff}^2\varepsilon^2 = n(n-1)\hbar^2\omega'^2$$

$$\varepsilon = \pm\sqrt{n(n-1)}\hbar\frac{\omega'}{2m}$$

$$= \pm\sqrt{n(n-1)}\hbar\omega_c \qquad (5.1.11)$$

These levels have been plotted as shown in **Fig5.1.1(A1.15)**. As is evident from the above relation the Landau energy level (resulting in the presence of magnetic field) in this case exhibit four-fold degeneracy for value of n greater than 2. The corresponding wavefunctions will be Hermite polynomials. If we now apply a magnetic field perpendicular to the bilayer plane, it will result in producing a potential difference between the two layers. Adding the (u/2 term) back to the Hamiltonian, one can immediately see it will result in shifting the energy eigen values by a factor proportional to u as shown in **Fig5.1.2.(A1.16)**

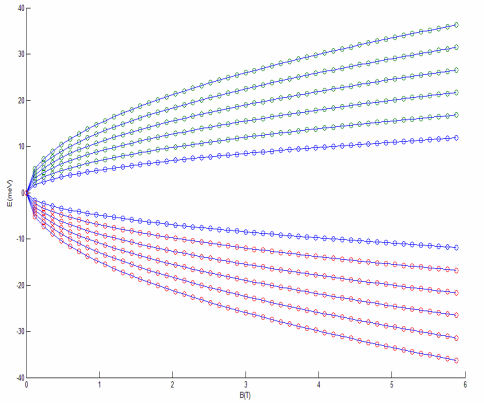

Fig5.1.1 showing E as a function of B for different energy levels. Note that as B increases the gap b/w the nth and the (n-1)th energy level increases.

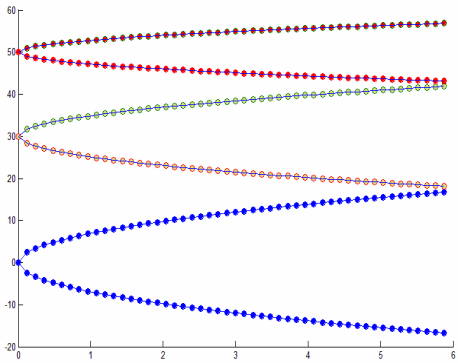

Fig5.1.2 .The reduction in gap b/w the electron and the hole state (+/-) reducing as the strength of the applied electric field increases. Different color corresponds to different values of electric field E.

4. Summary

To conclude we summarize the various results that have been obtained. As a first step, the conical dispersion relation of graphene single layer was established. This dispersion relation governs the unordinary electronic properties of graphene indicating the presence of low energy massless Dirac fermions near the K, K' valley. The dispersion relation was then recalculated to include the effects of confinement of the lattice on its properties. Two-type of edge structures exist in graphene resulting from its asymmetric unit vectors. The confinements effects for the zigzag edge showed a quantization in the band structure. A rather peculiar feature was observed for the case of arm-chair edge where the conducting properties of the layer were found to have a crisp dependence on the length L_x along the confined direction. Next we moved on to see the magnetic field effects on the graphene E-k characteristics for the infinite as well as the confined lattice. The magnetic field resulted in the Landau level quantization with a square root dependence of nth energy level on the integer n. In the presence of zigzag edge these states dispersed towards slightly higher energies near the edges which differed from the case of armchair edge where the dispersing edge states acquired a degeneracy of two near the edges.

Finally we studied the bilayer graphene system wherein we find out more intriguing properties including a peculiar Landau level characterization and the □ dependence in the dispersion relation. We derived an effective two-dimensional Hamiltonian to describe the system at low energies as well. Further investigations can be done on the same for tilted magnetic field where the concern would be to study the effect of the in-plane component of the magnetic field. Besides the effects of transverse electric field on the energy spectrum can be done for both the single layer as well as bilayer. Next stage could be device modeling out of the graphene layers requiring an analysis of graphene dot structures which would entail the electrostatic potential confinement of graphene electrons.

II. Experimental

1. Introduction

The determination and characterization of structure is a critical step in most solid-state research. Diffraction techniques using x-rays, neutrons or electron beam are widely employed to gain valuable information about materials at the atomic level. In this section we discuss the experimental aspects of graphene with respect to its synthesis from HOPG (Highly ordered pyrolitic graphite).The project aims at investigating and modeling the novel electronic properties of graphene and its synthesis from HOPG . In this part the TEM (Transmission Electron Microscopy) images of cleaved HOPG layers have been discussed in detail. A sample of HOPG was prepared by the process mentioned below. A sample of HOPG was prepared by the process mentioned below:

1.1 Sample preparation

The 5mm X 5mm HOPG sample was cleaved with the help of adhesive tapes and the obtained crystallites were dissolved in approximately 5ml ethanol solution. A perforated Cu substrate was then immersed in this solution. The solution was then sonicated to get deposition of HOPG flakes on the Cu substrate. A layer of size 2mm X 2mm was then deposited on to a carbonized Cu wafer to provide for the metallic contacts. The C coating was provided to act as an adhesive.

1.2 HRTEM imaging of the sample

The prepared HOPG sample on a Cu substrate was imaged using a HRTEM microscope. High Resolution Transmission Electron Microscopy (HRTEM) is an imaging mode of the transmission electron microscope (TEM) that allows the imaging of the crystallographic structure of a sample at an atomic scale. As opposed to conventional microscopy, HRTEM does not use amplitudes, i.e. absorption by the sample, for image formation. Instead, contrast arises from the interference in the image plane of the electron wave with itself. Due to our inability to record the phase of these waves, we generally measure the amplitude resulting from this interference, however the phase of the electron wave still carries the information about the sample and generates contrast in the image, thus the name phase-contrast microscopy. Each imaging electron interacts independently with the sample. Above the sample, the wave of an electron can be approximated as a plane wave incident on the sample surface. As it penetrates the sample, it is attracted by the positive atomic potentials of the atom cores, and channels along the atom columns of the crystallographic lattice. At the same time, the interaction between the electron wave in different atom columns leads to Bragg diffraction. The physics of electron scattering and electron microscope image formation are sufficiently well known to allow accurate simulation of electron microscope images.

1.3 Analysis of TEM images of HOPG

The following images were obtained using HRTEM tip on the sample of size 2mm X 2mm prepared on a Cu wafer.

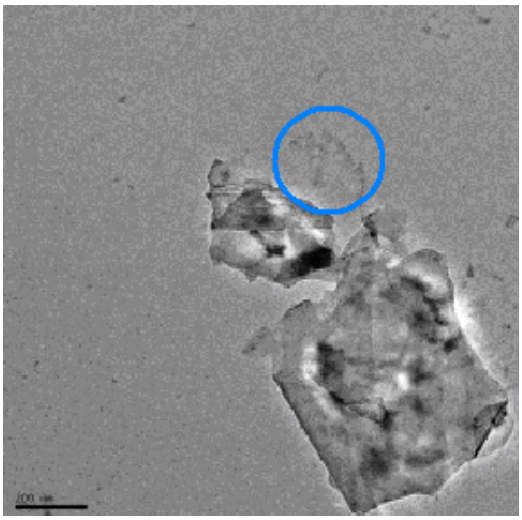

Fig1.3 a)Scale 200nm

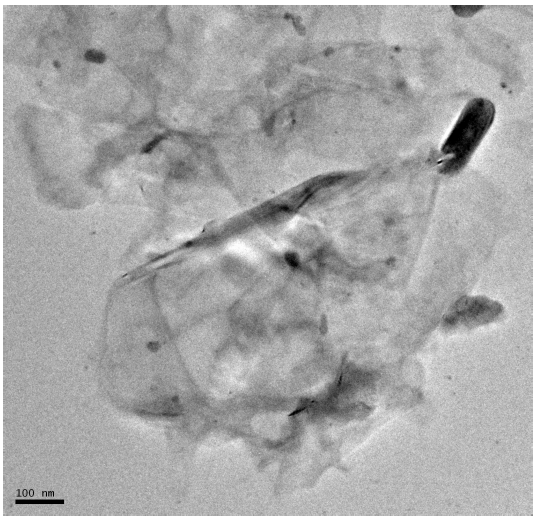

Fig1.3 b)Scale 200nm

Low magnification TEM images showing the surface morphology of the prepared HOPG sample. The bending of the layers of graphene sheets can be seen at the edges. The layers are creased with many folds, pleats and wrinkles. In the central part there is a homogeneous region without any feature at all. This might be quite close to monolayer graphene as is evident from some of the electron diffraction images showing a single periodicity[**22-23**].

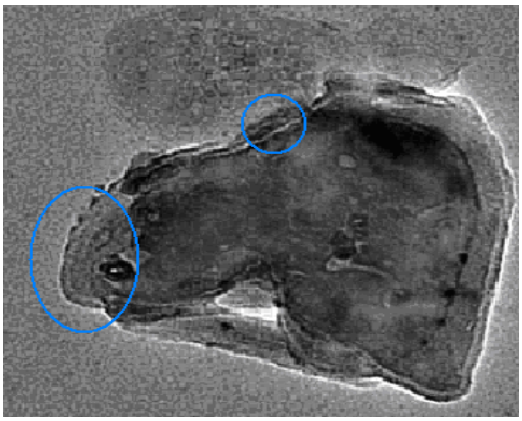

Fig1.4 a)scale 50 nm

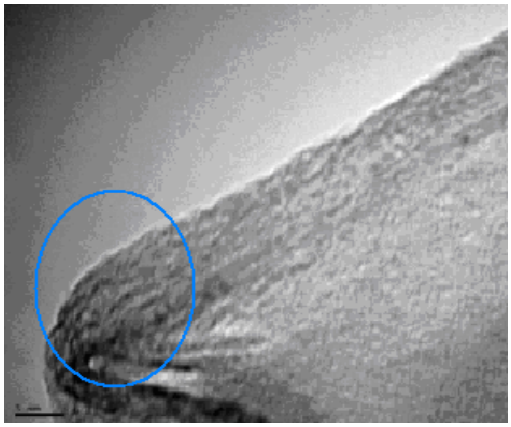

Fig1.4 b)scale 5 nm

The images shown in Fig.2 were obtained at a higher resolution by zooming in on the edges seen in the images shown in **Fig.1.3**. In **Fig1.4** a) layers can be seen sliding over the bottom most layer. The layered structure at the edge can be seen much more prominently in the image shown in **Fig1.4 b)** which is taken at a much smaller scale of 5 nm, quite comparable with the graphene hexagonal lattice dimension of 2.5 A^0 .

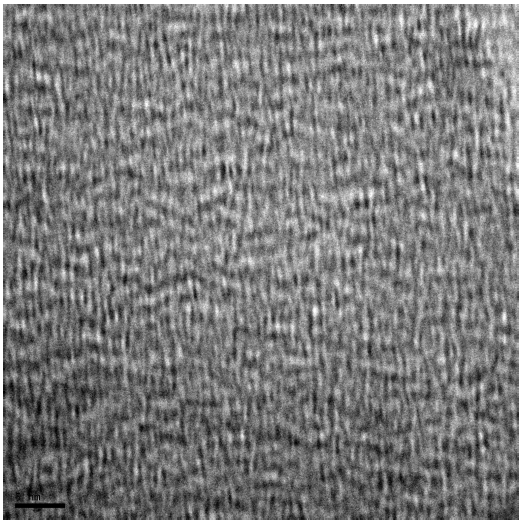

Fig1.5 a) scale 5 nm

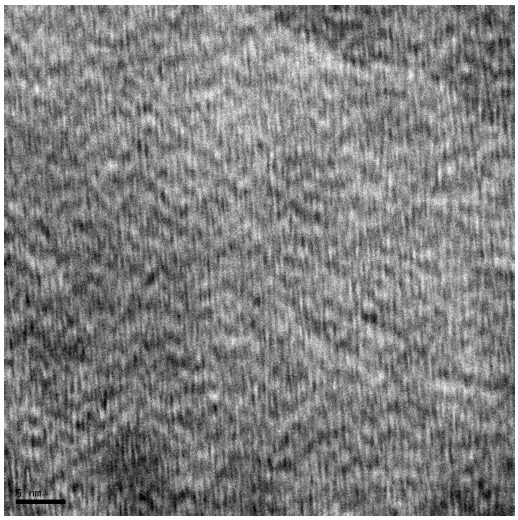

Fig1.5 b) scale 5nm

Fig 1.5 shows unfiltered image of the surface seen at a scale of 5 nm. Although a high frequency noise blurs the raw image, some kind of lattice structure can be recognized in both images. The above images were then processed by applying auto-correlation on them. Auto-correlation is precisely the cross-correlation of a signal with itself. It is useful for finding repeating patterns in an image, such as determining the presence of a periodic signal which has been buried under noise, or identifying the missing fundamental frequency in an image implied by its harmonic frequencies**.** The auto-correlated images were then Fourier transformed to look for the periodicities present in the image. **Fig 1.5a)** and **Fig.1.5b)** shows the auto-correlated and the FFT of the above images. A lattice periodicity of 2.52 A^0 and 1.17 A^0 are seen. The former corresponds to one of the lattice parameters of the hexagonal C-C lattice.

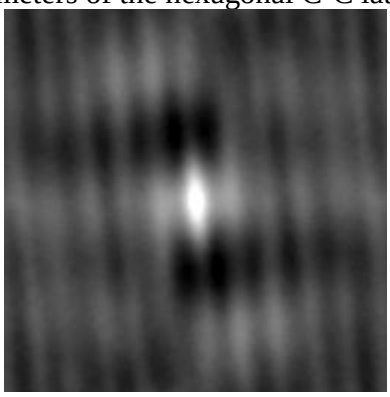

.

Fig1.5a)Auto-correlation of image shown in Fig1.4 Auto-correlation enhances the periodic feature -es by ignoring the noise in the image.

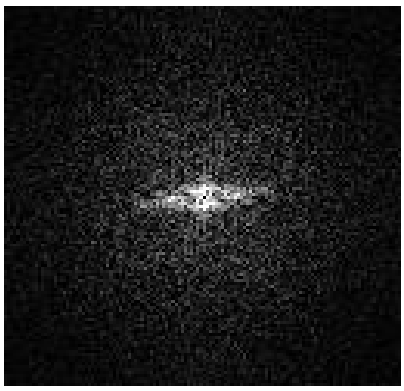

Fig1.5b)Fast Fourier Transform of the image shown in the left giving a blurred frequency spectrum

The following images were obtained by zooming in on the area marked in blue circle in **Fig1.1a**).Observing carefully the first micrograph in **Fig 1.6a)** one can notice different domain boundaries in the polycrystalline structure. Some of these domains show a very precise periodic structure.

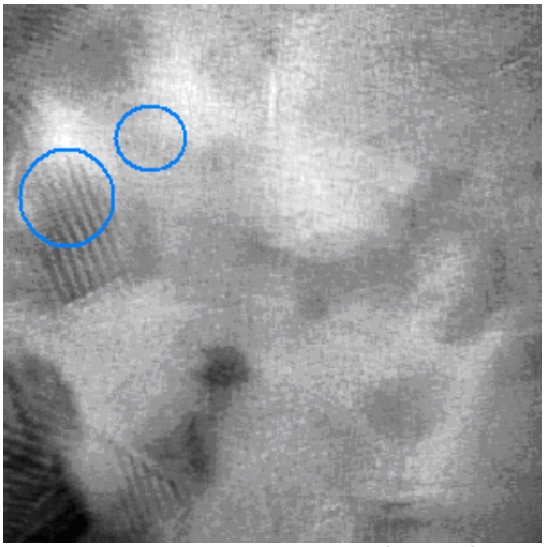

Fig1.6a) (scale 5 nm) micrograph of the surface showing different periodic and aperiodic domains.

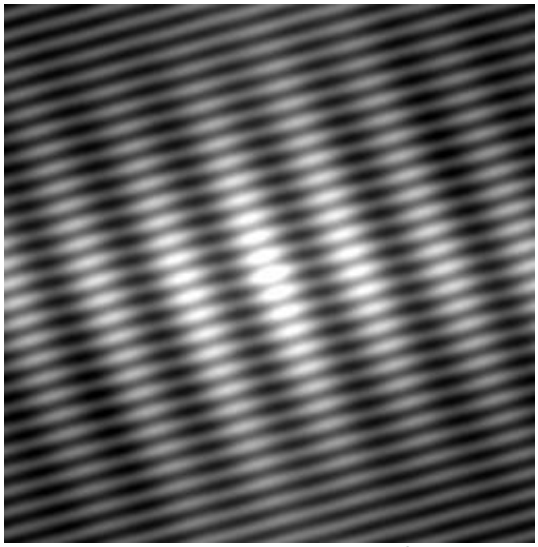

Fig1.6b) Auto-correlation on the part of the image 1.6a) encircled in blue.

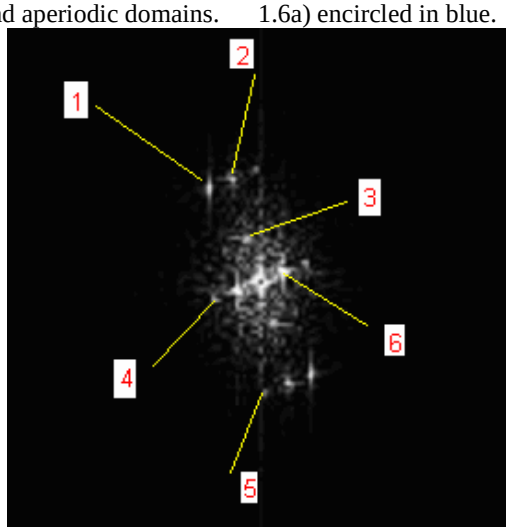

Fig 1.6c) showing the FFT of the image obtained in 1.6b)

Examination of **Fig.1.6c)** reveals 6 major spatial frequencies. These correspond to the following lattice parameters.

Point #	**Lattice parameter (nm)**
1	0.061567
2	0.04932
3	0.059434
4	0.317965
5	1.04723
6	0.260146

Following FFT images were obtained by zooming in on different part of the images.

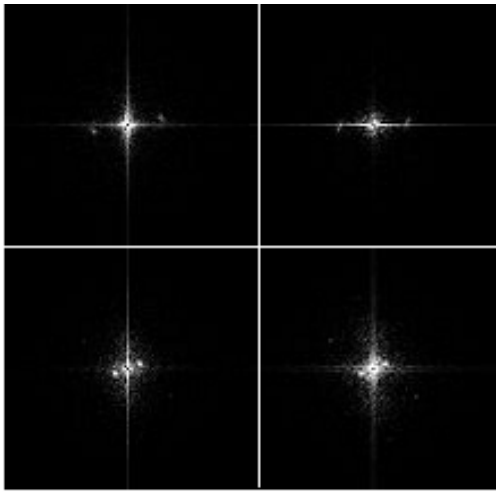

Fig1.7a) FFT at different crystallite domains

The corresponding lattice parameters come out to be .135, .127, 1.04, 1.04 nm for the shown images. The higher value lattice parameters might result from lattice imperfections like the stacking faults in HOPG or possibly due to random arrangement of layers. The periodicities of .26 nm and .135 nm are quite common along with weak higher order peaks. The periodicities reflected in the two bottom-most figures appear with almost same intensity in all the images. This is an indication of monolayer graphene since for a 2-D layer the obtained diffraction would be zero order, hence there would not be much alteration of the diffraction pattern for different incidence angle. This is not the case for a normal 3-D crystal where higher orders interfere with each other and the diffraction pattern varies with the angle of incidence. The experiment could be further modified to plot the intensity variation of the diffraction pattern with the tilt-angle. If a nominal TEM variation pattern is obtained, it would be a clear signature of the single layer graphene.

The idealized image of graphite surface is shown in **Fig1.8**. Green lattice corresponds to the top layer (A) and light green to next layer (B). Stacking sequence of HOPG is ABABAB,with periodicity of 1.42Å (C-C bond, blue cell) or the periodicity of the top layer alone. There is every third atom missing, so that primary cell is again hexagonal (red), but periodicity now 2.46Å.

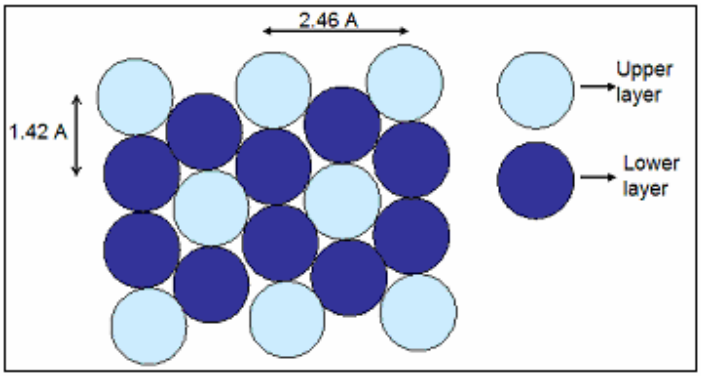

Fig1.8. Graphite lattice structure

Summary & Future Work

An attempt has been made to fabricate graphene on a Cu surface. HRTEM imaging had been used to analyze the obtained layers. While certain cues, hinting towards the presence of hexagonal lattice have been seen, no concrete evidence which signatures the presence of single graphene layer has been obtained. The work can be extended to theoretically simulate the electron diffraction of a single hexagonal layer which can be then be compared with the experimentally obtained electron micrograph. The simulation will need to take into account the realistic aspects of the process including substrate interference, electron beam energy range, corrugations on graphene surface to make the simulated patterns comparable with the HRTEM images. The obtained results might also find use in similar ultra-thin, transparent substrates.

References

[1]. The rise of graphene, A.K. Geim and K.S. Novoselov, Nature Materials 6, 183-191 (2007).

[2]. Numerical solution of the 1-D Schrödinger equation: Bloch Wavefunctions, Constantino A. Utreras Diaz, arXiv: physics/0503171 v2.

[3]. An analytical approach to understanding the structure of carbon nanotubes, Michael Campolongo (yet to appear in journal).

[4]. A novel choice of the graphene unit vectors, useful in zone folding computations, P. Marconcini, M. Macucci, Carbon 45 (2007) 1018-1024.

[5]. Electronic states of graphene nanoribbons studied with the Dirac equation, L.Brey and H.A. Fertig, Physical Review B 73, 235411.

[6]. Edge states and the quantised Hall effect in graphene, L.Brey and H.A.Fertig, Physical Review B 73, 195408 (2006).

[7]. Quantised Hall conductance, curent-carrying edge states and the existence of extended states in a two-dimensional disordered potential, B.I. Halperin, Physical Review B,Volume 25,Number 4.

[8]. Charge and spin transport at the quantum Hall edge of graphene, Dmitry A.Abanin, Patrick A.Lee, Leonid S. Levitov, Solid state communications 143(2007).

[9]. Magnetic and quantum confinemnt effects on electronic and optical properties of graphene ribbons, Y C Huang, C P Chang and M F Lin, Nanotechnology 18(2007) 495401.

[10]. Lattice-induced double-valley degeneracy lifting in graphene by a magnetic field, Igor A. Lukyanchuk and Alexandre M. Bratkovsky, arXiv:0707.0466v4, 2007.

[11]. Modulation effects of Landau levels in a monolayer graphene,JH Ho, Y H lai, Y H Chiu and M f Lin, Nanotechnology 1, 9(2008).

[12]. Two-dimensional gas of massless Dirac fermions in graphene. K.S. Novoselov, A.K. Geim, S.V. Morozov, D.Jiang, M.I. Katnelson, I. V. Grigorieva, S.V. Dubonos & A.A. Firsov, Nature 238, 04233.

[13]. Solvable linear potentials in the Dirac equation, Europhysics letters, 13(3), pp. 193-198.

[14]. Observation of Landau levels of Dirac fermions in graphite. Guohong and Eva Y. Andrei, Nature Physics 653, 13.

[15]. Spontaneous symmetry breaking and quantum Hall effect in graphene. Kun Yang, arXiv:cond-mat/0703757v3, 2008.

[16]. Dirac fermion confinement in graphene, N.M.R. Peres, A.H. Castro Neto and F. Guinea, Physical Review B 73, 241403.

[17]. Electron-electron interactions and the phase diagram of a bilayer graphene. Johan Nilsson, A.H. Castro Neto, N.M.R. Peres and F, Guniea, Physical Review B 73, 214418 (2006).

[18]. Gaped graphene bilayer: disorder and magnetic field effects, Eduardo V.Castro, N.M.R. Peres and J.M.B. Lopes dos Santos, Phys. Stat. Sol.(b) 244.

[19]. Unconventional quantum Hall effect and Berry's phase of 2pi in bilayer graphene. K.S. Novoselov, E.McCann, S.V. Morozov, V.I. Falko, M.I. Katsnelson, U.Zeitler, D.JIang, F.Schedin and A.K. Geim, Nature Physics, 245.

[20].Stacking characteristics of graphene shells in carbon nanotubes, X. Sun and C.H. Kiang, Physical Review B, Vol 54, 18.

[21]. The structure of suspended graphene sheets, Jannik c. Meyer, A.K. geim, M.I. Katnelson, T.J. Booth, S.Roth, Nature 446,05545.

[22]. Van der Waals interactions of the benzebe dimer: towards treatment of polycyclic aromatic hydrocarbon dimers, Svetla D. Chakrova and Elsabeth Schroeder, Applied physics report 2004-17.

[23]. Constructing Green functions of the Schroediner equation by elementary transformations, Gin-yih Tsaur, Jyhpyng Wang, American Journal of Physics, Vol. 74, No. 7, 601.

Appendix (Matlab codes)

A.1 (bloch wave)

```
a=2;
b=1;
nx=10;
ny=10;
n1=10;
A=[];
m=[];
for k=1:ny
for i=1:nx
    for j=4:n1-4
        m(((i-1)*10+j),((k-1)*10+j))= 1 ;
    end
end
end
for i = 1:nx*n1-4
 for j= 1:ny*n1-4
     Ax(i)=i;
     Ay(j)=j;
end
end
mesh(Ax,Ay,m)
u=[];


for i=1:nx
    for k=1:ny
        sum=0;
for j=1:n1
    for l=1:n1
    sum=sum + exp(complex(0,-i*2*pi/a*j/n1*a-
k*2*pi/b*l/n1*b))*m(j,l)*1/n1*a*1/n1*b;
    end
end
u(i,k)=sum/(a*b);
end
end

kix=2;
kiy=2;
m=9.109*10^(-31);
h=1.05457266*10^(-34);
%e=h^2*(ki*2*pi/a)^2/(2*m)
e=1;
```

```
i=1;
ct=0;

    for j=1:nx
        tex=h*h/(2*m)*(kix*2*pi/a-j*2*pi/a)^2 ;
        %x(j,j)=tex;
        for l=1:ny
        tey=h*h/(2*m)*(kiy*2*pi/a-l*2*pi/b)^2 ;
        x(j,l)=tey+tex;

          for k=j+1:nx
          x(j,l,k)=u(k-j,l);
          end

           for k=j+1:ny
         x(i,,k)=u(k-j,l);
          end


    end


for i=1:n-1
    b(1,i)=x(i,n);
end

for i=1:n-1
    for j=1:n-1
        c(i,j)=x(i,j);
    end
end

an=c/b;
sm=0;
n2=20;
for i=1:n2
    sm=0;
for j=1:n-1
    sm = sm + an(j,1)*exp(complex((i/n*a)*(ki-j)*2*pi/a));
end
sm = sm - exp(complex((i/n*a)*(ki-n)));
si(i)=sm;
end


for i=1:n2
    d(i)=i/n2*a;
```

```
end

scatter(d,real(si))
hold on
plot(d,real(si))
```

A.2 (wavefunction)

```
 Same as above take eigen vector instead of eigen value
```

A.3 (graphene e-k)

```
ans=[]*[];
a=1;
v=1;
n1=20;
emax=10;
emin=1;
del=(emax-emin)/n1;
gde=[];
gdk=[];
gde(1)= emin;
nk=20;

for k=2:n1
    gde(k)=gde(k-1)+ del;
end


for x=1:nk
    gk(x)=pi*(x-1)/(a*nk);
end

for x=1:nk
    the=gk(x)*a/2;
    for k = 1:n1
        e=gde(k);
        v=1;
si=[];
dsi=[];
n=10;
si(n)=1;
dsi(n)=0;

for i=1:n-1
    si(i+n)=si(i+n-1)+a/(2*n)*dsi(i+n-1);
    dsi(i+n)=dsi(i+n-1)-a/(2*n)*(e-v)*si(i+n-1);
```

```
    si(n-i)=si(-i+n+1)-a/(2*n)*dsi(-i+n+1);
    dsi(n-i)=dsi(-i+n+1)+a/(2*n)*(e-v)*si(-i+n+1);
end

si1=[];
dsi1=[];
a=1;
n=10;
si1(n)=0;
dsi1(n)=1;
for i=1:n-1
    si1(i+n)=si1(i+n-1)+a/(2*n)*dsi1(i+n-1);
    dsi1(i+n)=dsi1(i+n-1)-a/(2*n)*(e-v)*si1(i+n-1);

    si1(n-i)=si1(-i+n+1)-a/(2*n)*dsi1(-i+n+1);
    dsi1(n-i)=dsi1(-i+n+1)+a/(2*n)*(e-v)*si1(-i+n+1);
end

sum=0;
for i=1:2*n-1
    sum=sum+(si(i)^2*a/(2*n));
end

for i=1:2*n-1
    si(i)=si(i)/sqrt(sum);
end

sum=0;
for i=1:2*n-1
    sum = sum+((si1(i))*(si1(i))*a/(2*n));
end

for i=1:2*n-1
    si1(i)=si1(i)/sqrt(sum);
end

for i=1:19
    A(i)=i;
end


c2= si(1)*dsi1(1);
c1= si1(1)*dsi(1);

ans(x,k)=c1*(cos(the)^2)+ c2*(sin(the)^2);
```

```
    end
end

for i=1:nk
    ge(i)=gde(1);
    b=ans(i,1);
    for j=1:n1
        if(abs(ans(i,j))<b)
            ge(i)=gde(j);
            b=ans(i,j);
        end
    end
    ge(nk+i)=ge(i);
    gk(nk+i)=-gk(i);
end



scatter(gk,ge);close all;
clear all;
a=2;
n=10;
n1=10;
A=[];
m=[];

for i=1:n
    for j=4:n1-4
        m((i-1)*10+j)= 1 ;
    end
end

for i = 1:n*n1-4
    A(i)=i/(n*n1-4)*a;
end


%plot(A,m)
%hold on

u=[];a=2;
b=1;
nx=10;
ny=10;
n1=10;
A=[];
```

```
m=[];

for k=1:ny
for i=1:nx
    for j=4:n1-4
        m(((i-1)*10+j),((k-1)*10+j))= 1 ;
    end
end
end

for i = 1:nx*n1-4
 for j= 1:ny*n1-4
     Ax(i)=i;
     Ay(j)=j;
end
end

mesh(Ax,Ay,m)

u=[];


for i=1:nx
    for k=1:ny
        sum=0;
for j=1:n1
    for l=1:n1
    sum=sum + exp(complex(0,-i*2*pi/a*j/n1*a-
k*2*pi/b*l/n1*b))*m(j,l)*1/n1*a*1/n1*b;
    end
end
u(i,k)=sum/(a*b);
end
end

kix=2;
kiy=2;
m=9.109*10^(-31);
h=1.05457266*10^(-34);
%e=h^2*(ki*2*pi/a)^2/(2*m)
e=1;
i=1;
ct=0;

    for j=1:nx
        tex=h*h/(2*m)*(kix*2*pi/a-j*2*pi/a)^2 ;
        %x(j,j)=tex;
```

```
        for l=1:ny
        tey=h*h/(2*m)*(kiy*2*pi/a-l*2*pi/b)^2 ;
        x(j,l)=tey+tex;

          for k=j+1:nx
          x(j,l,k)=u(k-j,l);
          end

           for k=j+1:ny
         x(i,,k)=u(k-j,l);
          end


    end


for i=1:n-1
    b(1,i)=x(i,n);
end

for i=1:n-1
    for j=1:n-1
        c(i,j)=x(i,j);
    end
end

an=c/b;
sm=0;
n2=20;
for i=1:n2
    sm=0;
for j=1:n-1
    sm = sm + an(j,1)*exp(complex((i/n*a)*(ki-j)*2*pi/a));
end
sm = sm - exp(complex((i/n*a)*(ki-n)));
si(i)=sm;
end


for i=1:n2
    d(i)=i/n2*a;
end

scatter(d,real(si))
hold on
plot(d,real(si))
```

```
for i=1:n
    sum=0;
for j=1: n1
    sum=sum + exp(complex(0,-i*2*pi/a*j/n1*a))*m(j)*1/n1*a;
end
u(i)=sum/a;
end

ki=5;
m=9.109*10^(-31);
h=1.05457266*10^(-34);
%e=h^2*(ki*2*pi/a)^2/(2*m)
%e=1
i=1;
ct=0;

    for j=1:n
        te=h*h/(2*m)*(ki*2*pi/a-j*2*pi/a)^2 ;
        cx=te;
        ct=ct+1;
        x(j,j)=cx;
       for k=j+1:n
          cx=u(k-j);
          x(j,k)=cx;
          ct=ct+1;
       end
    end

[V,D] = eigs(x);
e=D(3);



sm=0;
n2=100;
for i=1:n2+1
    sm=0;
for j=1:n
    sm = sm + V(20+j)*exp(complex(0,(((i-1)/n2*a)*(ki-
j)*2*pi/a)));
end
si(i)=sm;
end


for i=1:n2+1
```

```
    d(i)=(i-1)/n2*a;
end

scatter(d,real(si))
hold on
plot(d,real(si))
```

A.4 (graphene wavefunction)

```
clear all
ab=1;
a=[];
b=[];
d=[];
e=[];
n=100;
c=1;
al=1;
be=1;
si=[];

for i=1:n
    for j=1:n
aa(i)=i;
bb(j)=j;
a(c)=i/n*3*pi-3*pi/2;
      b(c)=j/n*3*pi-3/2*pi;

d(c)=sqrt(1+4*cos(a(c)/2)*cos(sqrt(3)*b(c)/2)+4*cos(a(c)/2)
*cos(a(c)/2));
      e(c)=-d(c);
      cc(i,j)=d(c);
      t1=1+exp(complex(0,-
a(c)*ab*1.732))+exp(complex(0,a(c)*ab*1.732/2-b(c)*1.5*ab));
      t2=1+exp(complex(0,a(c)*ab*1.732))+exp(complex(0,-
a(c)*ab*1.732/2+b(c)*1.5*ab));
      m=[al-d(c),be*t1;be*t2,al-d(c)];
      [k,h]=eigs(m);
      c1(c)=k(1);
      c2(c)=k(2);
      si(i,j)= c1(c)*1 + c2(c)*2;
      c=c+1;
    end
end

    mesh(aa,bb,si)
    %hold on
```

```
   % scatter3(a,b,d,1)
    %hold on
    %scatter3(a,b,e,1)
```

A.5 (E-ky for zigzag edge)

```
clear all
close all
a0=pi;
n=100;
l=14*1.732*a0;

for j=1:5
    for i=1:n
    ky(i)=-2*pi/a0+4*i/n*pi/a0;
    f=@(x)ky(i)-x./tan(14*1.732*x.*1)

    kx(i,j)=fsolve(f,j/5);

    e1(i,j)=sqrt(kx(i,j)^2+ky(i)^2);
    e2(i,j)=-sqrt(kx(i,j)^2+ky(i)^2);
    end
end

for j=1:5
    for i=1:n
    kx(i)=kx(100*(j-1)+i);
    ee1(i)=e1(100*(j-1)+i);
    ee2(i)=e2(100*(j-1)+i);
    k(i)=sqrt(kx(i)^2+ky(i)^2);
    end
    plot(k,ee1)
    hold on
    plot(k,ee2)
    hold on
    plot(-k,ee1)
    hold on
    plot(-k,ee2)
    hold on
end


A.6
zigzag wave
```

A.7(E-k armchair)

```
clear all;
close all;
n=100;
n1=50;
for j=1:5
    for i=1:n
        ky(i)=.9+.9*i/n;
        e1(i)=sqrt(j-1);
        e2(i)=-sqrt(j-1);
        e11(i)=sqrt(j-1);
        e22(i)=-sqrt(j-1);
    end

    for k=1:n1
        ky(n+k)=1.8+k/n1*.3;
        e1(n+k)=5*(ky(n+k)-ky(n))^2+e1(n);
        e2(n+k)=-5*(ky(n+k)-ky(n))^2-e1(n);
        if(j==1)
        e11(n+k)=5*(ky(n+k)-ky(n))^2+e1(n);
        e22(n+k)=-5*(ky(n+k)-ky(n))^2-e1(n);
        else
        e11(n+k)=e1(n)+4*(ky(n+k)-1.82)^2-.0004;
        e22(n+k)=-(e1(n)+4*(ky(n+k)-1.82)^2-.0004);
        end
    end

      for k=1:n1
        ky(n+n1+k)=ky(1)-k/n1*.3;
        e1(n+n1+k)=5*(ky(n+k)-ky(n))^2+e1(n);
        e2(n+n1+k)=-5*(ky(n+k)-ky(n))^2-e1(n);
        if(j==1)
        e11(n+n1+k)=5*(ky(n+k)-ky(n))^2+e1(n);
        e22(n+n1+k)=-5*(ky(n+k)-ky(n))^2-e1(n);
        else
        e11(n+n1+k)=e1(n)+4*(ky(n+k)-1.82)^2-.0004;
        e22(n+n1+k)=-(e1(n)+4*(ky(n+k)-1.82)^2-.0004);
        end
    end
    scatter(ky,e1)
    hold on
    scatter(ky,e2)
    hold on
    scatter(ky,e11)
    hold on
    scatter(ky,e22)
    hold on
end
```

A.8(Armchair edge 2)

Same as above, change L as mentioned in the text.

A.9 (zigzag edge in a magnetic field)

```
clear all
close all
a=1.5;
n=100;
l=1;
b=50;
n1=0;
for i=1:n
    k(i)= (2*(n-n1-i))/n*a;
end

for i=1:n
    %si(i)=((exp(k(i)-5))*(8*(k(i)-b)^3-12*(k(i)-b)));
    si(i)=1/k(i)*exp(k(i))^2*(k(i)^2-4);
end

for i=1:n
    si1(i)=si(n+1-i)+200;
end

plot(k,si1/900)
hold on
scatter(k,si1/900)
```

A.10 (armchair edge in magnetic field)

```
clear all;
close all;
n=100;
n1=50;
for j=1:5
    for i=1:n
        ky(i)=.9+.9*i/n;
        e1(i)=sqrt(j-1);
        e2(i)=-sqrt(j-1);
        e11(i)=sqrt(j-1);
        e22(i)=-sqrt(j-1);
    end

    for k=1:n1
```

```
        ky(n+k)=1.8+k/n1*.3;
        e1(n+k)=5*(ky(n+k)-ky(n))^2+e1(n);
        e2(n+k)=-5*(ky(n+k)-ky(n))^2-e1(n);
        if(j==1)
        e11(n+k)=5*(ky(n+k)-ky(n))^2+e1(n);
        e22(n+k)=-5*(ky(n+k)-ky(n))^2-e1(n);
        else
        e11(n+k)=e1(n)+4*(ky(n+k)-1.82)^2-.0004;
        e22(n+k)=-(e1(n)+4*(ky(n+k)-1.82)^2-.0004);
        end
    end

      for k=1:n1
        ky(n+n1+k)=ky(1)-k/n1*.3;
        e1(n+n1+k)=5*(ky(n+k)-ky(n))^2+e1(n);
        e2(n+n1+k)=-5*(ky(n+k)-ky(n))^2-e1(n);
        if(j==1)
        e11(n+n1+k)=5*(ky(n+k)-ky(n))^2+e1(n);
        e22(n+n1+k)=-5*(ky(n+k)-ky(n))^2-e1(n);
        else
        e11(n+n1+k)=e1(n)+4*(ky(n+k)-1.82)^2-.0004;
        e22(n+n1+k)=-(e1(n)+4*(ky(n+k)-1.82)^2-.0004);
        end
    end
    scatter(ky,e1)
    hold on
    scatter(ky,e2)
    hold on
    scatter(ky,e11)
    hold on
    scatter(ky,e22)
    hold on
end
```

A.11 (two well potential)

```
close all
clear all
for i=1:100
    x(i)=-1+i/100;
    y(i)=.1+(x(i)+.5)^2;
end
%scatter(x,y)
for i=1:100
    x(100+i)=i/100;
    y(100+i)=-.1+(x(100+i)-.5)^2;
end
```

```
scatter(x,y)
```

A.12 (armchair edge in magnetic field E-k)

```
clear all;
close all;
n=100;
n1=50;
for j=1:5
    for i=1:n
        ky(i)=.9+.9*i/n;
        e1(i)=sqrt(j-1);
        e2(i)=-sqrt(j-1);
        e11(i)=sqrt(j-1);
        e22(i)=-sqrt(j-1);
    end

    for k=1:n1
        ky(n+k)=1.8+k/n1*.3;
        e1(n+k)=5*(ky(n+k)-ky(n))^2+e1(n);
        e2(n+k)=-5*(ky(n+k)-ky(n))^2-e1(n);
        if(j==1)
        e11(n+k)=5*(ky(n+k)-ky(n))^2+e1(n);
        e22(n+k)=-5*(ky(n+k)-ky(n))^2-e1(n);
        else
        e11(n+k)=e1(n)+4*(ky(n+k)-1.82)^2-.0004;
        e22(n+k)=-(e1(n)+4*(ky(n+k)-1.82)^2-.0004);
        end
    end

      for k=1:n1
        ky(n+n1+k)=ky(1)-k/n1*.3;
        e1(n+n1+k)=5*(ky(n+k)-ky(n))^2+e1(n);
        e2(n+n1+k)=-5*(ky(n+k)-ky(n))^2-e1(n);
        if(j==1)
        e11(n+n1+k)=5*(ky(n+k)-ky(n))^2+e1(n);
        e22(n+n1+k)=-5*(ky(n+k)-ky(n))^2-e1(n);
        else
        e11(n+n1+k)=e1(n)+4*(ky(n+k)-1.82)^2-.0004;
        e22(n+n1+k)=-(e1(n)+4*(ky(n+k)-1.82)^2-.0004);
        end
    end
    scatter(ky,e1)
    hold on
    scatter(ky,e2)
    hold on
    scatter(ky,e11)
```

```
    hold on
    scatter(ky,e22)
    hold on
end
```

A.13 (E-k bilayer)

```
 u =.2;
 v=8;
 v3=.1*v;
 si=-1;
 y1=.39;
 n=100;

 for i=1:100
     kx(i)=-pi+i/n*2*pi;
     ky(i)=-pi+i/n*2*pi;
 end

 for i=1:100
     for j=1:100
       ki=complex(kx(i),ky(j));
       kki=complex(kx(i),-ky(j));
       mat=[u/2 v3*ki 0 v*kki; v3*kki -u/2 v*ki 0; 0 v*kki
-u/2 si*y1; v*ki 0 si*y1 u/2 ];
       en=eigs(mat);
       e(i,j)=abs(en(1));
     end
 end

 surf(kx,ky,e)
 hold on
 %surf(kx,ky,-e)
 shading interp
```

A.14

```
Same as above (contour plot)
```

A.15

```
clear all
close all
for j=4:4
    for i=1:50
        b(i)=(i-1)/50*6;
        e(i)=2*sqrt(j*j-j)*sqrt(b(i));
    end
```

```
    scatter(b,e)
    hold on
    scatter(b,-e)
    hold on
plot(b,e)
    hold on
    plot(b,-e)
    hold on

end

j=3;
for i = 1:50
e(i)=2*sqrt(j*j-j)*sqrt(b(i));
end
u=0;
temp=e-u;
e=30+temp;
e1=30-temp;
scatter(b,e)
    hold on
    scatter(b,e1)
    hold on
plot(b,e)
    hold on
    plot(b,e1)
    hold on

    j=2;
for i = 1:50
e(i)=2*sqrt(j*j-j)*sqrt(b(i));
end
u=0;
temp=e-u;
e=50+temp;
e1=50-temp;
scatter(b,e)
    hold on
    scatter(b,e1)
    hold on
plot(b,e)
    hold on
    plot(b,e1)
    hold on
```

A.16

```
Same as above with parameters changed as mentioned in text.
```